Physica 125A (1984) 163–196
North-Holland, Amsterdam

# LONG-TIME TAILS IN A QUANTUM LORENTZ GAS

W. HOOGEVEEN* and J.A. TJON

*Institute for Theoretical Physics, Princetonplein 5, P.O. Box 80.006, 3508 TA Utrecht, The Netherlands*

Received 8 September 1983

The long-time behaviour of the velocity autocorrelation function (VACF) in a quantum Lorentz gas is investigated using both tetradic and double contour methods. The two classes of most divergent diagrams in the double contour analysis, called ladders and stars, are summed explicitly for the case of separable interactions. The ladders lead to the ringsum long-time tail. The stars give rise to a curious $t^{-d/2}$-tail which is of quantum-mechanical nature. Moreover these diagrams yield an additional contribution to the classical $t^{-(d/2+1)}$-tail which might explain the discrepancy between the observed and predicted long-time tail coefficient. Extending the star diagrams to the class of ladders of stars, the $t^{-d/2}$-tail is shown to be removed for the two-dimensional case. Quantum corrections to the long time tail coefficient arising from the tetradic ring digrams are studied in two and three dimensions. A repeated ringsum expression for the VACF has been evaluated numerically for all times to study the cage effect and appearance of the algebraic long-time tail.

## 1. Introduction

One of the remarkable findings of classical kinetic theory is the fact that the simple Lorentz gas exhibits algebraic decay of time dependent correlation functions and nonanalytic density dependence of transport coefficients like normal fluids[1,2]). In particular Ernst and Weijland[3]) obtained a negative $t^{-(d/2+1)}$ long-time tail by considering a ringsum expression for the velocity autocorrelation function (VACF) in a $d$-dimensional hard sphere Lorentz gas. This type of algebraic decay is indicated by molecular dynamics studies[4,5,6]) as well. The coefficient of the long-time tail found in this manner appears to be at least two times as large as the one predicted. In a previous paper[7]), hereafter to be referred to as I, we have considered a quantum version of the Lorentz gas. It has been found that the leading order divergence of the two scatterer term in the usual density expansion of the Laplace transformed VACF is changed only trivially if the system is described quantum mechanically. This implies that the leading order nonanalytic density behaviour of the quantum system is essentially similar to that of the classical system[7,8]). The long-time behaviour of the VACF is changed more drastically by quantum effects. It has been shown[7,9]) that bound state processes give rise to correlations falling off proportional to $t^{-1}\exp(i\omega_0 t)$ for long times. A quantum-mechanical ringsum expression for the VACF also leads to a negative

* Present address: Royal Dutch/Shell Exploration and Production Laboratory, 2280 AB Rijswijk, The Netherlands.

$t^{-(d/2+1)}$ long time tail. For the three-dimensional hard sphere system, it has been noted[8]) that the coefficient of the long-time tail consists of the classical term and some quantum corrections that become important at low energies. There exists a class of diagrams in the perturbation expansion of the Laplace transformed VACF, which leads after resummation to a logarithmically divergent contribution to the VACF in the $d = 2$ case. This divergence is regarded as a signal that the wave function of the light particle is localised for any two-dimensional system with arbitrarily small disorder[10]). Translated into time language this implies that there exists a certain class of diagrams which generates a $t^{-d/2}$ long time tail. Recently, it has been shown[11]) that this tail can also be obtained by resummation of the leading order parts of the so-called special diagrams in the tetradic analysis.

In this paper we study the time dependence of the VACF for the quantum Lorentz gas in two and three dimensions. We'll use both double contour and tetradic methods, as discussed in I. In section 2 the double contour analysis is given. First of all we define a diagrammatic representation which turns out to be very convenient for separable interactions. Then we consider the algebraic tails produced by the classes of most divergent diagrams. In particular the class of so-called symmetric star diagrams leads to a $t^{-(d/2)}$-tail in accordance with the results of Kirkpatrick and Dorfman[11]). As a byproduct we find that the asymmetric star diagrams lead to an additional contribution to the classical $t^{-(d/2+1)}$-tail which has precisely the same strength as the classical ringsum contribution[3]). As a result this may explain the discrepancy between the observed and predicted long time tail coefficients[4-6]). In section 3 we discuss in which manner the $t^{-d/2}$-tail can be influenced by less divergent diagrams if $d = 2$. It provides an example how this $t^{-1}$-behaviour is replaced by a faster decreasing one for asymptotic long time. In view of the $\rho$-dependence of the less divergent diagrams the $t^{-1}$-dependence however would still be seen on a certain time scale for sufficiently low density. This result does not seem to yield additional support to the assumption made in a previous letter[12]) that the long time behaviour is determined by the hydrodynamic mode only. The tetradic analysis is carried out in section 4. We start reviewing briefly some of the properties of the tetradic operators. The naive divergences that appear in the straight-forward density expansion of the VACF are removed by means of a Dyson–Zwanzig[13]) inversion. Subsequently, the quantum corrections to the long time tail coefficient arising from the ring diagrams are studied in two and three dimensions for the case of separable S-wave interactions. In section 5 we introduce a scalar inversion method alternatively to the Dyson–Zwanzig procedure, in order to formulate a repeated ringsum expression for the VACF that we have evaluated numerically for all times in a semi classical approximation. In particular we find that the times for which the asymptotic $t^{-(d/2+1)}$-tail holds may be longer than has been studied up to now in molecular dynamics simulations. The paper closes with some concluding remarks.

## 2. Double contour analysis of the velocity autocorrelation function

In this section we start repeating some of the definitions concerning the double contour formalism given in I. Subsequently, we introduce a diagrammatic representation in order to study the long time behaviour of the VACF.

The Lorentz gas consists of a light particle that moves in a $d$-dimensional box of volume $\Omega$ containing $N$ scatterers fixed at random positions $\boldsymbol{R}^N \equiv (\boldsymbol{R}_1, \ldots, \boldsymbol{R}_N)$. The Laplace transform of the VACF, $\hat{S}(\epsilon)$ is defined by

$$\hat{S}(\epsilon) = \int_0^\infty \mathrm{d}t \, \exp(-\epsilon t) \langle \boldsymbol{P} \cdot \boldsymbol{P}^{(N)}(t) \rangle \,, \tag{2.1}$$

where $\boldsymbol{P}$ is the momentum operator for the light particle and

$$\boldsymbol{P}^{(N)}(t) = \exp(\mathrm{i}H_N t) \boldsymbol{P} \exp(-\mathrm{i}H_N t) \,, \tag{2.2}$$

$H_N$ is the $N$-scatterer Hamiltonian. This expression has to be considered in the thermodynamic limit, i.e. $N \to \infty$ at fixed scatterer density $\rho = N/\Omega$. To determine the average of any operator $A$ one must take the trace in the light particle Hilbert space and integrate over all scatterer positions which is indicated by a $\overline{\phantom{x}}$,

$$\langle A \rangle = \mathrm{Tr}[\overline{\exp(-\beta H_N) A}] / \mathrm{Tr}[\overline{\exp(-\beta H_N)}] \,. \tag{2.3}$$

Related to $\hat{S}(\epsilon)$ we define the energy-dependent correlation function $\hat{S}(E, \epsilon)$ by

$$\hat{S}(\epsilon) = \left[ \int \mathrm{d}\boldsymbol{p} \, \exp(-\beta p^2) p^2 \hat{S}(p^2, \epsilon) \right] \Big/ \int \mathrm{d}\boldsymbol{p} \, \exp(-\beta p^2) \,. \tag{2.4}$$

The cluster functions $s_n(E, \epsilon)$ are obtained from the formal cluster expansion of $\hat{S}(E, \epsilon)$

$$\hat{S}(E, \epsilon) = \epsilon^{-1} + \sum_{n=1}^{\infty} s_n(E, \epsilon) \rho^n \,. \tag{2.5}$$

After the application of a Watson transformation to eq. (2.1), cf. I(2.10), and assuming that the interactions do not support bound states we obtain the following expression for $\hat{S}(\epsilon)$:

$$\hat{S}(\epsilon) = [-2\pi \mathrm{Tr}\, \overline{\exp(-\beta H_N)}]^{-1} \oint \mathrm{d}z \, \exp(-\beta z) \, \mathrm{Tr}[\overline{\boldsymbol{P} G_N(z - \mathrm{i}\epsilon) \cdot \boldsymbol{P} G_N(z)}] \,. \tag{2.6}$$

The $z$-contour encloses the positive real axis in a counter-clockwise direction. It has been found in eq. I(3.16) that only the upper half of the contour contributes to the singular behaviour, so that we replace $z$ by $E + \frac{1}{2}\mathrm{i}\epsilon$ and integrate over all

positive values of $E$. This leads to the following expression for the energy-dependent correlation function:

$$\hat{S}(E,\epsilon) = a_d \Omega^{-N-1} \operatorname{Tr}[\overline{\boldsymbol{P}G_N(z_-)\cdot \boldsymbol{P}G_N(z_+)}]\,,$$
$$a_d = \frac{2(2\pi)^{d-1}}{p^d \omega_d}\,, \tag{2.7}$$

where $p=\sqrt{E}$, $z_\pm = E \pm \frac{1}{2}\mathrm{i}\epsilon$ and $\omega_d = \int \mathrm{d}\hat{p}$. In this expression all statistical correlations have been ignored.

A diagrammatic representation of the binary collision expansion for $Q_n(E,\epsilon)$, which is defined by

$$Q_n(E,\epsilon) = \operatorname{Tr}[\overline{\boldsymbol{P}G_n(z_-)\cdot \boldsymbol{P}G_n(z_+)}] \tag{2.8}$$

is treated in detail in appendix A. This expansion arises from the binary collision expansion of both $n$-scatterer Green's functions in terms of free propagators $G_0$ and one-scatterer collision operators $T_1$. From the cluster expansion of the r.h.s. of eq. (2.7) it follows that the $n$th cluster function can be expressed in terms of the connected diagrams of $Q_n$,

$$s_n(E,\epsilon) = a_d \Omega^{-1} Q_{n,\mathrm{c}}(E,\epsilon)\,. \tag{2.9}$$

By connected we mean that all $n$ scatterers participate in a given diagram. Some comments on the combinatorics are made in appendix A. The analysis simplifies considerably if we use a separable $T_1$-operator of the familiar form, eq. I(3.2),

$$T_1^{(j)}(z) = \lambda \Delta^{-1}(z) \exp(\mathrm{i}\boldsymbol{R}_j\cdot\boldsymbol{P})|g\rangle\langle g|\exp(-\mathrm{i}\boldsymbol{R}_j\cdot\boldsymbol{P})\,,$$
$$\Delta(z) = 1 - \lambda\langle g|G_0(z)|g\rangle\,. \tag{2.10}$$

To find the contribution to $Q_{n,\mathrm{c}}$ of any connected diagram, as shown for instance in fig. 1, one has to start labelling all dots representing $T$-operators. Dots connected by dashed lines must be labelled equally. Moreover each diagram

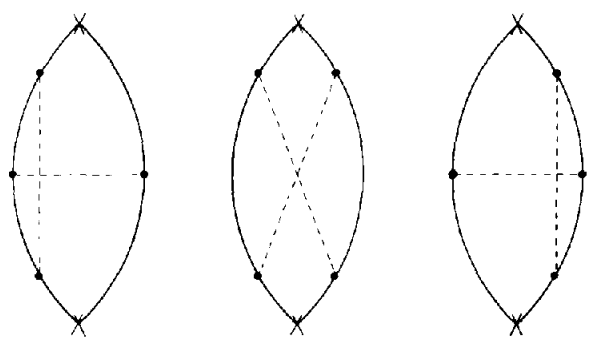

Fig. 1. Divergent two-scatterer diagrams.

contains two crosses representing the operators $\boldsymbol{P}$. Going around the diagram in a clockwise direction the solid line segments have to be replaced according to the following rules:

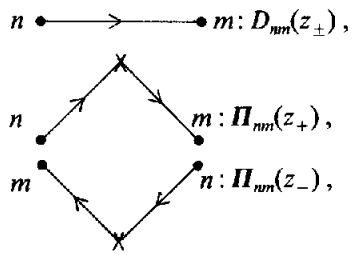


(2.11)

where

$$D_{nm}(z_\pm) = D(\boldsymbol{R}_{nm}, z_\pm) = [\lambda/\Delta(z_\pm)]\langle g|\exp(\mathrm{i}\boldsymbol{R}_{nm}\cdot\boldsymbol{P})G_0(z_\pm)|g\rangle\,. \tag{2.12}$$

$\boldsymbol{R}_{nm} = \boldsymbol{R}_n - \boldsymbol{R}_m$, the distance between scatterers $n$ and $m$. Sometimes we'll omit the scatterer indices of the $D$-functions if the $\boldsymbol{R}$-dependence is obvious. The complex energy argument is $z_-$ resp. $z_+$ if the segment is on the left resp. the right arc of the diagram. For large scatterer separations $R$ the asymptotic behaviour of $D(z\pm)$ is proportional to $(\sqrt{R})^{1-d}\times\exp(-R\sqrt{-z_\pm})$, cf. eqs. I(3.10) and I(A.17). The $\Pi$-vectors are defined by

$$\boldsymbol{\Pi}_{nm}(z_\pm) = \boldsymbol{\Pi}(\boldsymbol{R}_{nm}, z_\pm) = [\lambda/\Delta(z_\pm)]\langle g|\exp(-\mathrm{i}\boldsymbol{R}_{nm}\cdot\boldsymbol{P})G_0(z_-)\boldsymbol{P}G_0(z_+)|g\rangle\,, \tag{2.13}$$

or in terms of $D$-functions

$$\boldsymbol{\Pi}_{nm}(z_\pm) = \frac{-1}{\epsilon\Delta(z_\pm)}\frac{\partial}{\partial\boldsymbol{R}_{nm}}[\Delta(z_+)D_{nm}(z_+) - \Delta(z_-)D_{nm}(z_-)]\,. \tag{2.14}$$

The asymptotic form of $\boldsymbol{\Pi}$ in the large $R$-region follows from the behaviour of the $D$-functions stated above. Assuming the interactions to be isotropic, the $\boldsymbol{\Pi}$'s are anti-symmetric in the scatterer indices while the $D$'s are symmetric. Consequently, if, in a given diagram, there are two dots connected by a dashed line such that in between them there is only a cross and an arbitrary number of isolated dots, then this particular diagram vanishes. The class of diagrams without any dashed line leads to the naive divergences of the $s_n$'s, describing the uncorrelated collision sequences (see appendix A). The simplest correlated contributions are given by the two-scatterer diagrams as shown in fig. 1 and involve four $T$-operators. They yield the following contribution to $s_2$:

$$a_d\Omega^{-1}\int \mathrm{d}\boldsymbol{R}_1\,\mathrm{d}\boldsymbol{R}_2[\boldsymbol{\Pi}_{12}(z_+)\cdot\boldsymbol{\Pi}_{21}(z_-)][D_{12}^2(z_+) - D_{12}(z_-)D_{12}(z_+) + D_{12}^2(z_-)]\,. \tag{2.15}$$

For the two-dimensional system these are the logarithmically divergent contributions to the second cluster functions as discussed in I(3.17).

Next, we locate those diagrams that are as divergent as the classical ring diagrams. Firstly, we note that adding an isolated dot to any divergent diagram leads asymptotically to multiplication with a factor of $\mathcal{O}(\rho\epsilon^{-1})$, as can readily be seen from eq. (2.23) below. Hence, we only have to consider diagrams not containing isolated dots; we will call them skeletons. The simplest $n$-scatterer skeletons are built out of $2n$ pairwise coupled dots. The most singular ones are those for which all oscillatory factors of the $\boldsymbol{\Pi}$'s and $D$'s cancel at large scatterer separations $R$. As a rule of thumb the type of divergence of these simplest skeletons can be determined by noting that the $n$-scatterer configuration space grows proportional to $(R^d)^{n-1}$, while the integrand is typically damped proportional to $(\sqrt{R})^{-2n(d-1)}$ in this case, which means that the most singular, simplest $n$-scatterer skeletons are as divergent as the classical ring diagrams. Every other skeleton will be less divergent, either because there are oscillating factors remaining, or because there is additional damping due to the presence of extra line segments. It follows that only two classes of skeletons satisfy all these requirements; they are shown in fig. 2 and fig. 3 and referred to as ladders and stars. Note by comparing these figures and fig. 1 that the two-scatterer skeletons have been overcounted here.

All stars and ladders can be summed explicitly due to the use of separable

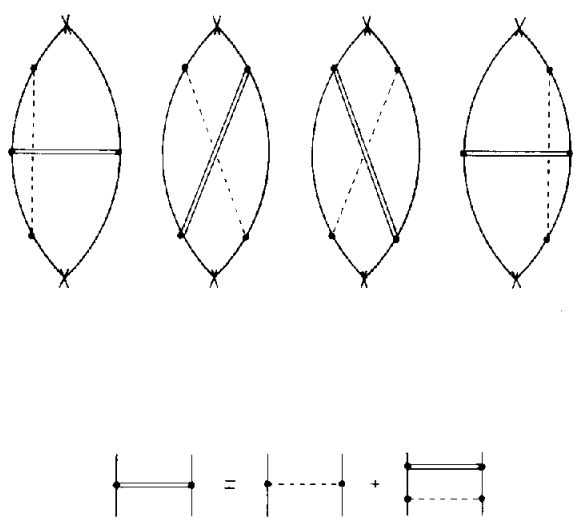

Fig. 2. Ladder skeletons.

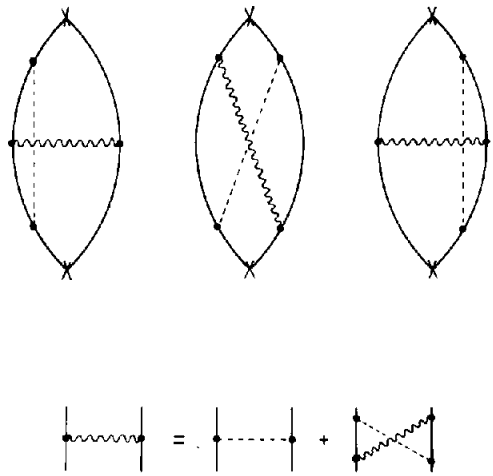

Fig. 3. Star skeletons.

interactions. For the ladder contribution to $\hat{S}(E,\epsilon)$ we have to consider

$$\rho^2 \int \mathrm{d}\boldsymbol{R}_1\, \mathrm{d}\boldsymbol{R}_2\, \mathrm{d}\boldsymbol{R}_3 [\boldsymbol{\Pi}_{23}(z_+)\cdot\boldsymbol{\Pi}_{31}(z_-)] F_{12}$$
$$\times [D_{32}(z_+)D_{13}(z_+) - D_{31}(z_-)D_{32}(z_+) - D_{23}(z_+)D_{13}(z_+) + D_{31}(z_-)D_{23}(z_-)]\,,$$

with

$$F_{12} = \rho D_{12}(z_-)D_{21}(z_+) + \rho^2 \int \mathrm{d}\boldsymbol{R}_4\, D_{14}(z_-)D_{42}(z_-)D_{24}(z_+)D_{41}(z_+)$$
$$+ \rho^3 \int \mathrm{d}\boldsymbol{R}_4\, \mathrm{d}\boldsymbol{R}_5\, D_{14}(z_-)D_{45}(z_-)D_{52}(z_-)D_{25}(z_+)D_{54}(z_+)D_{41}(z_+) + \cdots . \tag{2.16}$$

The integrals in eq. (2.16) are of a simple convolution type. As a result the series can be summed by Fourier transformation. We get

$$\begin{aligned} F_{12} &= (2\pi)^{-d} \int \mathrm{d}\boldsymbol{q}\, \exp(\mathrm{i}\boldsymbol{q}\cdot\boldsymbol{R}_{12})[1-\rho U_\epsilon(q)]^{-1} - \delta(\boldsymbol{R}_{12}) \\ &= (2\pi)^{-d} \int \mathrm{d}\boldsymbol{q}\, \exp(\mathrm{i}\boldsymbol{q}\cdot\boldsymbol{R}_{12})[\rho U_\epsilon(q)][1-\rho U_\epsilon(q)]^{-1}\,, \end{aligned} \tag{2.17}$$

where

$$U_\epsilon(q) = \int \mathrm{d}\boldsymbol{R}\, \exp(\mathrm{i}\boldsymbol{q}\cdot\boldsymbol{R}) D(z_-)D(z_+)\,. \tag{2.18}$$

This enables us to write down the contribution of all ladders $L(E,\epsilon)$ to $\hat{S}(E,\epsilon)$ in a closed form,

$$\begin{aligned} L(E,\epsilon) = {} & \rho^2 a_d \Omega^{-1} \int \mathrm{d}\boldsymbol{R}_1\, \mathrm{d}\boldsymbol{R}_2\, \mathrm{d}\boldsymbol{R}_3 [\boldsymbol{\Pi}_{23}(z_+)\cdot\boldsymbol{\Pi}_{31}(z_-)] \\ & \times [D_{32}(z_+)D_{13}(z_+) - D_{31}(z_-)D_{32}(z_+) - D_{23}(z_-)D_{13}(z_+) \\ & + D_{31}(z_-)D_{23}(z_-)](2\pi)^{-d} \int \mathrm{d}\boldsymbol{q}\, \exp(\mathrm{i}\boldsymbol{q}\cdot\boldsymbol{R}_{12})[1-\rho U_\epsilon(q)]^{-1} \\ & + \rho^2 a_d \Omega^{-1} \int \mathrm{d}\boldsymbol{R}_1\, \mathrm{d}\boldsymbol{R}_3 [\boldsymbol{\Pi}_{13}(z_+)\cdot\boldsymbol{\Pi}_{31}(z_-)] D_{31}(z_-)D_{31}(z_+)\,. \end{aligned} \tag{2.19}$$

The double counting of the symmetric two scatterer diagram is removed by the last term in this expression. This correction, however, will be omitted since it only gives rise to an exponentially decaying contribution to the VACF. In the remaining expression for $L$ the $\boldsymbol{R}$-integrals factorise

$$L(E,\epsilon) = a_d(2\pi)^{-d} \int \mathrm{d}\boldsymbol{q}[1-\rho U_\epsilon(q)]^{-1}[\boldsymbol{V}_\epsilon(\boldsymbol{q},z_-)\cdot\boldsymbol{V}_\epsilon(\boldsymbol{q},z_+)]\,, \tag{2.20}$$

where

$$\boldsymbol{V}_\epsilon(\boldsymbol{q},z_\pm) = \rho \int \mathrm{d}\boldsymbol{R}\, \boldsymbol{\Pi}(z_\pm)[D(z_+)-D(z_-)]\exp(\mathrm{i}\boldsymbol{q}\cdot\boldsymbol{R})\,. \tag{2.21}$$

The contribution $A(E,\epsilon)$ to $\hat{S}(E,\epsilon)$ of all stars with at least three scatterers can be derived analogously,

$$\begin{aligned} A(E,\epsilon) = {} & \rho^2 a_d \Omega^{-1} \int \mathrm{d}\boldsymbol{R}_1\, \mathrm{d}\boldsymbol{R}_2\, \mathrm{d}\boldsymbol{R}_3 \int \frac{\mathrm{d}\boldsymbol{q}}{(2\pi)^d}\left[\frac{\rho U_\epsilon(q)}{1-\rho U_\epsilon(q)}\right] \\ & \times \{[\boldsymbol{\Pi}_{31}(z_-)\cdot\boldsymbol{\Pi}_{23}(z_+)][D_{31}(z_-)D_{23}(z_+) + D_{32}(z_-)D_{13}(z_-)]\exp(\mathrm{i}\boldsymbol{q}\cdot\boldsymbol{R}_{12}) \\ & + [\boldsymbol{\Pi}_{31}(z_-)\cdot\boldsymbol{\Pi}_{31}(z_+)]D_{12}(z_-)D_{12}(z_+)\exp(\mathrm{i}\boldsymbol{q}\cdot\boldsymbol{R}_{23})]\}\,. \end{aligned} \tag{2.22}$$

Finally, the skeletons have to be dressed with isolated points, this is done by replacing all free propagators $G_0$ by renormalised propagators $\tilde{G}_0$ which are defined by

$$\tilde{G}_0(z) = [z - H_0 - \rho\bar{T}_1(z)]^{-1}\,. \tag{2.23}$$

If we are dealing with the renormalised version of any other function, this will be indicated by a ~ as well.

We may now consider the longtime behaviour which is induced by $\tilde{L}$ and $\tilde{A}$. The classical algebraic long-time tail results from the fact that the origin of the complex $\epsilon$-plane appears to be a branchpoint of a left-hand cut once the most

singular correlated collision sequences are taken into account. This is not an exact property of the summed ladders and stars. The position of the cut is given by those values of $c$ for which the $[1-\rho\tilde{U}_c(q)]$ denominators in eqs. (2.20) and (2.22) vanish for real positive values of $q$. In order to get the branchpoint at the origin one should have $\rho\tilde{U}_0(0)=1$, this equality however only holds to the lowest order in $\rho$. It follows from the general analysis of Maleev and Toperverg[14]) that the corresponding shift of the branchpoint is an artefact introduced by the fact that we are considering restricted classes of diagrams. If we neglect these higher order effects the denominators turn out to have the familiar hydrodynamic form

$$1-\rho\tilde{U}_c(q)\sim\epsilon_0^{-1}(E)[\epsilon+\gamma(E)q^2]\,, \tag{2.24}$$

with

$$\gamma(E)=\frac{4\pi E}{\omega_d\epsilon_0(E)}\left(\frac{4}{3}\right)^{d-2} \tag{2.25}$$

and

$$\begin{aligned}&\epsilon_0(E)=\pi\omega_d p^{d-2}\bar{\rho}\sigma,\quad \bar{\rho}=(2\pi)^d\rho,\quad \sigma=|T_1(p,p^2+\mathrm{i}0)|^2\,,\\ &T_1(p,z)=\lambda g^2(p)\Delta^{-1}(z)\qquad(\text{cf. eq. (2.10)})\,.\end{aligned} \tag{2.26}$$

Some details on the underlying asymptotic analysis of $\tilde{U}$ can be found in appendix B. The small $q$ behaviour of the numerators of $\tilde{L}$ and $\tilde{A}$ follows from simple symmetry arguments. It is readily seen that the numerator of $\tilde{L}$ is $\mathcal{O}(q^2)$ since both $\tilde{V}$-vectors vanish linearly if $q\to 0$. Hence it follows that the dressed ladders give rise to a $t^{-(d/2+1)}$ long-time contribution to the VACF. In appendix B it is shown that to the leading order in the density this is just the classical tail, as obtained after resummation of the ring diagrams. Here we only state the resulting contribution to $S(E,t)$,

$$\begin{aligned}&S_L(E,t)\sim\frac{1}{2}\left(\frac{3}{4}\sqrt{\pi}\right)^{d-2}\zeta_{12}(\gamma t)^{-(d/2+1)}\,,\\ &\zeta_{12}=-\frac{4\pi^2E(16/9)^{d-2}}{\omega_d\bar{\rho}\epsilon_0^2}\,.\end{aligned} \tag{2.27}$$

Analogously, it can be shown that the first two terms of the r.h.s. of eq. (2.22) for $\tilde{A}$ have a similar small $q$ behaviour. Hence these asymmetric stars give rise to a $t^{-(d/2+1)}$ tail as well. In appendix B the explicit form of this contribution to the VACF has been derived, the result is given by

$$\begin{aligned}&S_{A_a}(E,t)=\frac{1}{2}\left(\frac{3}{4}\sqrt{\pi}\right)^{d-2}(\zeta_{12}+\zeta_a)(\gamma t)^{-(d/2+1)}\,,\\ &\zeta_a=\frac{8(16/9)^{d-2}\pi p^4}{p^d\omega_d^2\epsilon_0^3}\,.\end{aligned} \tag{2.28}$$

Comparing eqs. (2.27) and (2.28) it appears that the term with $\zeta_{12}$ of the above expression gives rise to an additional contribution to the classical long-time coefficient, so that the total result would be in better agreement with the molecular dynamics simulations[5,6]). The remaining term of eq. (2.28) has a different cross section dependence. Furthermore $\zeta_a$ can be shown to become large compared to $\zeta_{12}$ if the energy is decreased.

The last term on the r.h.s. of (2.22) corresponds to the symmetric star diagrams $\tilde{A}_s$. Its numerator no longer vanishes if $q \to 0$, so that it leads to a $t^{-(d/2)}$-tail[11]). In particular for $d = 2$ we have $\tilde{A}_s(E, \epsilon) = \mathcal{O}(\log \epsilon)$. The asymptotic analysis of $\tilde{A}_s$ is dealt with in appendix B and it turns out that for long times $\tilde{A}_s$ yields the following contribution to $S(E, t)$:

$$S_{A_s}(E, t) \sim -\frac{(\sqrt{\pi}/2)^{d-2}}{\pi p^{d-2} \epsilon_0 (\gamma t)^{d/2}}. \tag{2.29}$$

This completes the discussion of the asymptotic behaviour of the stars and ladders.

## 3. Resummation of ladders of symmetric stars

If the true asymptotic behaviour of the VACF would be described by the most divergent diagrams, eq. (2.29) would lead to the non-existence of the diffusion coefficient in the case of $d = 2$. In this section we discuss the resummation of a certain class of less divergent diagrams which removes the corresponding $\log \epsilon$ divergence of the symmetric stars, indicating the importance of the less divergent diagrams for the two-dimensional system.

The set of diagrams considered are the ladders of symmetric stars as shown in fig. 4. The general expression of the $n$-star skeleton contribution to $\hat{S}(E, \epsilon)$ is given by

$$\begin{aligned} A_n(E, \epsilon) = \rho^n a_d \Omega^{-1} \int \mathrm{d}\boldsymbol{R}^n \, \mathrm{d}\boldsymbol{R}^{n'} \int \mathrm{d}\boldsymbol{q}^{n-1} \, \mathrm{d}\boldsymbol{q}^{(n-1)'} \, \mathrm{d}\boldsymbol{k}^n \, \mathrm{d}\boldsymbol{p}_+ \, \mathrm{d}\boldsymbol{p}_- (2\pi)^{-3nd} \\ \times \exp \mathrm{i} \Big\{ \boldsymbol{R}_{n'n} \cdot \boldsymbol{p}_+ + \boldsymbol{R}_{1'1} \cdot \boldsymbol{p}_- + \sum_{i=1}^{n} \boldsymbol{R}_{ii'} \cdot \boldsymbol{k}_i \\ + \sum_{i=1}^{n-1} (\boldsymbol{r}_{i',i+i} \cdot \boldsymbol{q}_i + \boldsymbol{R}_{(i+1)',i} \cdot \boldsymbol{q}_{i'}) \Big\} \\ \times [\hat{\boldsymbol{\Pi}}(\boldsymbol{p}_+, z_+) \cdot \boldsymbol{\Pi}(\boldsymbol{p}_-, z_-)] \left[ \prod_{i=1}^{n-1} \hat{D}(\boldsymbol{q}_i, z_-) \hat{D}(\boldsymbol{q}_{i'}, z_+) \right] \prod_{i=1}^{n} \delta_\epsilon(\boldsymbol{k}_i) . \end{aligned} \tag{3.1}$$

A few notational remarks:

– we have used primed and unprimed indices as shown in fig. 4;

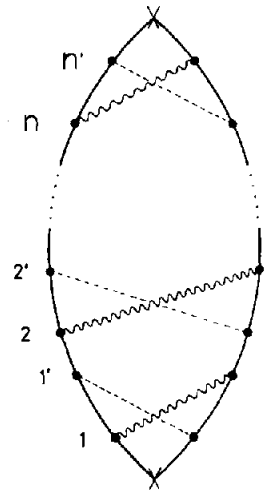


Fig. 4. Repeated star skeletons.

– $\mathrm{d}\boldsymbol{R}^n \equiv \mathrm{d}\boldsymbol{R}_1 \ldots \mathrm{d}\boldsymbol{R}_n$, the other integration elements are defined analogously;

– $a\hat{}$ over any function indicates the Fourier transform of it, where $\hat{f}(\boldsymbol{q}) \equiv \int \mathrm{d}\boldsymbol{R} \exp(\mathrm{i}\boldsymbol{q}\cdot\boldsymbol{R}) f(\boldsymbol{R})$, hence

$$\hat{\boldsymbol{\Pi}}(\boldsymbol{p}, z) = (2\pi)^d \boldsymbol{p} T_1(p, z)[(z_+ - p^2)(z_- - p^2)]^{-1}, \tag{3.2}$$

$$\hat{D}(\boldsymbol{q}, z) = (2\pi)^d T_1(q, z)(z - q^2)^{-1}, \tag{3.3}$$

$$\hat{\delta}_\epsilon(\boldsymbol{k}) = \rho U_\epsilon(k)[1 - \rho U_\epsilon(k)]^{-1}, \tag{3.4}$$

where $T(p, z) \equiv \langle \boldsymbol{p} | T(z) | \boldsymbol{p} \rangle$. The $2n$ $\boldsymbol{R}$-integrals can be carried out giving $(2n-1)$ delta functions

$$\begin{aligned}\int \mathrm{d}\boldsymbol{R}^n \mathrm{d}\boldsymbol{R}^{n'} \exp \mathrm{i}\{\ldots\} &= (2\pi)^{d(2n-1)} \Omega \delta(\boldsymbol{q}_1 - \boldsymbol{q}_{1'}) \ldots \delta(\boldsymbol{q}_{n-1} - \boldsymbol{q}_{(n-1)'}) \\ &\times \delta(\boldsymbol{k}_1 - \boldsymbol{q}_1 - \boldsymbol{p}_-)\delta(\boldsymbol{k}_2 - \boldsymbol{q}_2 - \boldsymbol{q}_{1'}) \ldots \delta(\boldsymbol{k}_{n-1} - \boldsymbol{q}_{n-1} - \boldsymbol{q}_{(n-2)'}) \\ &\times \delta(\boldsymbol{k}_n - \boldsymbol{p}_+ - \boldsymbol{q}_{(n-1)'}).\end{aligned} \tag{3.5}$$

After dressing up the skeletons it is readily seen that for $d = 2$ the small $\epsilon$ behaviour of $\tilde{A}_n(E, \epsilon)$ is determined by the values of the integrand in the small $k_i$ $(i = 1, \ldots, n)$ region, where the $n$-star diagrams turn out to form a geometric series

$$\tilde{A}_n(E, \epsilon) \sim (-\rho)^n a_d \int \frac{\mathrm{d}\boldsymbol{p}'}{(2\pi)^d} [\hat{\tilde{\boldsymbol{\Pi}}}(\boldsymbol{p}', z_+)\cdot\hat{\tilde{\boldsymbol{\Pi}}}(\boldsymbol{p}', z_-)][\hat{\tilde{D}}(\boldsymbol{p}', z_+)\hat{\tilde{D}}(\boldsymbol{p}', z_-)]^{n-1} \bar{l}_\epsilon^n \tag{3.6}$$

where $l_\epsilon \equiv \int \mathrm{d}\boldsymbol{k}\, (2\pi)^{-d} \hat{\delta}_\epsilon(\boldsymbol{k})$. Note that this factorisation does not occur in three dimensions. By combining eqs. (3.6) and (3.2)–(3.4) it is found that

$$\sum_{n=1}^{\infty} \tilde{A}_n(E,\epsilon) \sim -\rho a_d (2\pi)^d \int \mathrm{d}\boldsymbol{p}' p'^2 |T_1(p', z_+)|^2 \tilde{l}_\epsilon$$
$$\times [(\tilde{z}_- - p'^2)(\tilde{z}_+ - p'^2)\{(\tilde{z}_- - p'^2)(\tilde{z}_+ - p'^2) + (2\pi)^{2d}\rho |T_1(p', z_+)|^2 \tilde{l}_\epsilon\}]^{-1}, \quad (3.7)$$
$$\tilde{z} \equiv z - \bar{\rho} T_1(p', z).$$

For small $\rho$ and $\epsilon$, the integrand of eq. (3.7) has simple poles if $p'^2 = \tilde{p}'^2_\pm$ or if $p'^2 = \tilde{\tilde{p}}'^2_\pm$, where

$$\tilde{p}'^2_\pm = E \pm \tfrac{1}{2}\mathrm{i}\epsilon_0,$$
$$\tilde{\tilde{p}}'^2_\pm = E \pm \tfrac{1}{2}\mathrm{i}\sqrt{\epsilon_0^2 + 4\rho(2\pi)^{2d}|T_1(p, z_+)|^2 \tilde{l}_\epsilon}. \quad (3.8)$$

The leading order behaviour of $\Sigma \tilde{A}_n$ is given by the residues at these poles

$$\sum_{n=1}^{\infty} \tilde{A}_n(E,\epsilon) \sim -\epsilon_0^{-1} + [\epsilon_0^2 + 4(2\pi)^{2d}\rho |T_1(p, z_+)|^2 \tilde{l}_\epsilon]^{-1/2}. \quad (3.9)$$

From this expression we see that the logarithmic divergence of $\tilde{A}_1(E,\epsilon)$ is removed in this way. It should be noted however in view of the density dependence of $\tilde{l}_\epsilon$ that the $t^{-1}$-behaviour may dominate on a certain time scale, but according to eq. (3.9) this $t$-dependence will subsequently be replaced by a faster decreasing one for asymptotic long times. Moreover it follows from eqs. (A.3) and (3.9) that the contributions to $\hat{S}(E,\epsilon)$ of the uncorrelated collisions and the ladders of symmetric stars cancel in the limit $\epsilon \to 0$. It is suggestive to ascribe this cancellation to the localisation of the light particle wave function in the two-dimensional system. In appendix C we argue that the removal of the log $\epsilon$-divergence can already be seen from the asymptotic form of the 4-point function of ladders of symmetric stars.

## 4. Long-time behaviour from the tetradic analysis

We start reviewing some of the definitions for the tetradic analysis given in I. Subsequently, some properties and a Dyson–Zwanzig[13]) procedure for the removal of the naive divergences will be discussed. Instead of the Heisenberg representation we now use a Liouville operator to describe the time evolution of the light particle momentum operator, cf. eq. (2.2)

$$\boldsymbol{P}^{(N)}(t) = \exp(\mathrm{i}\mathscr{L}_N t)\boldsymbol{P}. \quad (4.1)$$

The tetradic matrix elements of $\mathscr{L}_N$ can readily be expressed in terms of the $N$-scatterer Hamiltonian, cf. I(4.3)–I(4.5),

$$(\boldsymbol{p}, \boldsymbol{q}|\mathscr{L}_N|\boldsymbol{p}', \boldsymbol{q}') = \langle \boldsymbol{p}|H_N|\boldsymbol{p}'\rangle \delta(\boldsymbol{q} - \boldsymbol{q}') - \delta(\boldsymbol{p} - \boldsymbol{p}')\langle \boldsymbol{q}'|H_N|\boldsymbol{q}\rangle. \quad (4.2)$$

The Green's function $\mathscr{G}_N$ and the collision operator $\mathscr{W}_N$ are related to $\mathscr{L}_N$ by the usual expressions

$$\mathscr{G}_N(\chi) = (\chi - \mathscr{L}_N)^{-1} = \mathscr{G}_0(\chi) + \mathscr{G}_0(\chi)\mathscr{W}_N(\chi)\mathscr{G}_0(\chi)\,. \tag{4.3}$$

As discussed in I(4.13), $\mathscr{W}_1$ is the generalisation of the classical Lorentz–Boltzmann operator. The explicit expression for $\mathscr{W}_1$ is given in appendix D, eq. (D.1). An important property of the classical collision operator is the fact that it gives zero when acting on a constant mode. Viewed from the quantum-mechanical analysis this hydrodynamic property is a direct consequence of the fact that the unit operator is a zero eigen state for each tetradic collision operator. This can be proven at once from the definition (4.3) and the fact that $\mathscr{L}_n\hat{1} = 0$, for all $n$. In terms of tetradic matrix elements this implies

$$\int \mathrm{d}\boldsymbol{p}'\,(\boldsymbol{p},\boldsymbol{q}|\mathscr{W}_n(\chi)|\boldsymbol{p}',\boldsymbol{p}') = 0\,. \tag{4.4}$$

for all values of $\chi$. Eq. (4.4) can also be derived directly from eq. (D.1) using the generalised optical theorem for the $n$-scatterer $T$-operator

$$T_n(z) - T_n^\dagger(z) = T_n(z)[G_0(z) - G_0^\dagger(z)]T_n^\dagger(z)\,. \tag{4.5}$$

The higher $\mathscr{W}_n$'s ($n \geq 2$) are expanded in a binary collision series that can be represented diagrammatically. To illustrate this let us consider the expansion of $\mathscr{W}_2$,

$$\mathscr{W}_2^{(12)} = (1 + P_{12})(\mathscr{W}_1^{(1)} + \mathscr{W}_1^{(1)}\mathscr{G}_0\mathscr{W}_1^{(2)} + \mathscr{W}_1^{(1)}\mathscr{G}_0\mathscr{W}_1^{(2)}\mathscr{G}_0\mathscr{W}_1^{(1)} + \cdots)\,. \tag{4.6}$$

$P_{12}$ permutes the superscripts indicating scatterer positions. In fig. 5 we show the first three terms of $(2!)^{-1}\mathscr{G}_0\bar{\mathscr{W}}_2\mathscr{G}_0$ that follow from eq. (4.6). In order to find the operator expression for a given diagram one has to start labeling the scatterers indicated by circles ○. Going around the diagram subsequently, one has to write a $\mathscr{G}_0$ for each line segment — and a $\mathscr{W}_1^{(i)}$ each time a scatterer labelled ($i$) is encountered. Finally, all scatterer positions are to be integrated out. The Laplace transform of the VACF, eq. (2.1), can be written in terms of the operators we have just defined,

$$\hat{S}(\epsilon) = -\mathrm{i}\langle \boldsymbol{P}\mathscr{G}_N(\chi)\boldsymbol{P}\rangle, \qquad \chi \equiv -\mathrm{i}\epsilon\,. \tag{4.7}$$

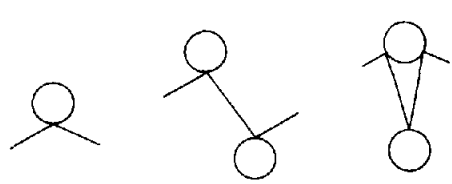

Fig. 5. The first three terms of the binary collision expansion of $\mathscr{W}_2$.

The naive divergences appear if one carries out a cluster expansion of $\mathscr{G}_N$. They can be removed using the fact that $\tilde{\mathscr{G}}'_N \equiv \Omega^{-N}\tilde{\mathscr{G}}_N$ satisfies a Dyson equation

$$\tilde{\mathscr{G}}'_N = \mathscr{G}_0 + \rho\mathscr{G}_0\hat{\Sigma}\tilde{\mathscr{G}}'_N, \tag{4.8}$$

where $\hat{\Sigma}$ is the sum of all multiple connected diagrams, of which we mention the first few below

$$\hat{\Sigma} = \bar{\mathscr{W}}_1 + \rho\int \mathrm{d}\boldsymbol{R}_1\mathscr{W}_1^{(1)}\mathscr{G}_0\bar{\mathscr{W}}_1\mathscr{G}_0\mathscr{W}_1^{(1)} + \cdots. \tag{4.9}$$

By formally solving eq. (4.8) we obtain an expression for $\hat{S}(\epsilon)$ which is of the well-known Zwanzig form

$$\hat{S}(\epsilon) = -\mathrm{i}\,\mathrm{Tr}[\exp(-\beta H_0)\boldsymbol{P}(\chi - \mathscr{L}_0 - \rho\hat{\Sigma})^{-1}\boldsymbol{P}]/\mathrm{Tr}[\exp(-\beta H_0)]. \tag{4.10}$$

In deriving this expression we have again ignored the statistical correlations. The first term of the $\hat{\Sigma}$-kernel describes the uncorrelated or binary collision sequences; the remaining, or correlated diagrams are denoted by $\rho\mathscr{R} \equiv \hat{\Sigma} - \bar{\mathscr{W}}_1$. Eq. (4.10) is studied by expanding $\tilde{\mathscr{G}}_N$ in terms of this $\mathscr{R}$,

$$\hat{S}(\epsilon) = -\mathrm{i}\,\mathrm{Tr}[\exp(-\beta H_0)\boldsymbol{P}\{\tilde{\mathscr{G}}_0 + \rho\tilde{\mathscr{G}}_0\mathscr{R}\tilde{\mathscr{G}}_0 + \cdots\}\boldsymbol{P}]/\mathrm{Tr}[\exp(-\beta H_0)], \tag{4.11}$$

where

$$\tilde{\mathscr{G}}_0(\chi) = (\chi - \mathscr{L}_0 - \rho\bar{\mathscr{W}}_1)^{-1}. \tag{4.12}$$

The limiting form of the binary contribution to $\hat{S}(E, \epsilon)$ for small $\epsilon$ can readily be derived, the result is given by

$$\tilde{S}_{\mathrm{b}}(E, \epsilon) \sim [\epsilon - \mathrm{i}\bar{\rho}\langle \boldsymbol{p}|\hat{\boldsymbol{P}}\mathscr{W}_1(-\mathrm{i}0^+)\hat{\boldsymbol{P}}|\boldsymbol{p}\rangle]^{-1}. \tag{4.13}$$

From the limiting form of $\mathscr{W}_1$, eq. (D.2) we immediately recover the exponentially decaying contribution of the simplest connected double diagrams as discussed in appendix A, cf. eq. (A.3). The next term on the r.h.s. of eq. (4.11) leads to the algebraically decaying long-time contributions.

As in the classical model[2]), there are several types of diagrams contained in $\mathscr{R}$ which yield divergent contributions to $\hat{S}$ if $\epsilon \to 0$. In fig. 6 we give some examples of the ring and special diagrams which are the two most divergent classes. The leading order behaviour of the ring diagrams, which correspond to the ladders of the previous section, is essentially the same for both classical and quantum-mechanical systems[7]). The cross sections that appear in the classical result are simply replaced by the quantum mechanical ones. The special diagrams behave qualitatively differently (see appendix E). In particular it has been shown in ref. 11 that a resummation of the leading order parts of these diagrams leads to the $t^{-d/2}$-tail of the symmetric stars, eq. (2.29), which is of quantum-mechanical nature.

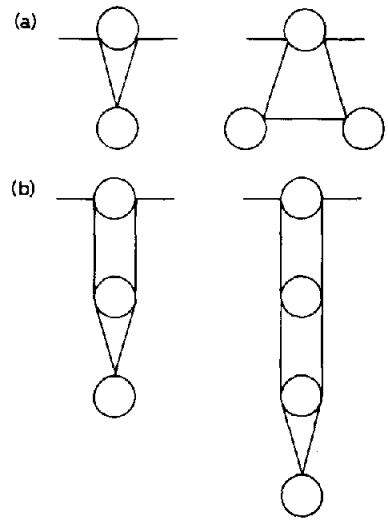


Fig. 6. Some examples of ring diagrams (a); and special diagrams (b).

We now turn to study in some detail the long-time behaviour of the ring diagrams for the case of separable S-wave interactions. The ring approximation corresponds to replacing $\mathscr{R}$ in eq. (4.11) by

$$\mathscr{R}_r = \int \mathrm{d}\boldsymbol{R}_1 \mathscr{W}_1^{(1)}(\chi - \mathscr{L}_0 - \rho \bar{\mathscr{W}}_1)^{-1} \mathscr{W}_1^{(1)} . \tag{4.14}$$

For convenience we extend our notation. Firstly, we introduce an operator $\Lambda_q$ which is closely related to $\bar{\mathscr{W}}_1$,

$$\langle \boldsymbol{p}, \boldsymbol{q} | \bar{\mathscr{W}}_1(\chi) | \boldsymbol{p}', \boldsymbol{q}' \rangle = (2\pi)^d \delta(\boldsymbol{q} - \boldsymbol{q}') \langle \boldsymbol{p} | \Lambda_{\boldsymbol{q}}(\epsilon) | \boldsymbol{p}' \rangle . \tag{4.15}$$

In order to get a simple delta function after averaging out the scatterer coordinates, we used a new tetradic basis which is related to the one we used previously in the following manner:

$$|\boldsymbol{p}, \boldsymbol{q}\rangle \equiv |\boldsymbol{p} + \tfrac{1}{2}\boldsymbol{q}, \boldsymbol{p} - \tfrac{1}{2}\boldsymbol{q}) . \tag{4.16}$$

The explicit matrix elements of $\Lambda_q$ are given in eq. (D.3). The constant mode acts as a zero eigen state of $\Lambda_0$ for all values of $\epsilon$, i.e.

$$\int \mathrm{d}\boldsymbol{p}' \langle \boldsymbol{p} | \Lambda_0(\epsilon) | \boldsymbol{p}' \rangle = 0 , \tag{4.17}$$

which is a direct consequence of the general hydrodynamic property, eq. (4.4). Hence $\Lambda_q$ has a hydrodynamic eigen state with vanishing eigen value if $q \to 0$. Using eqs. (4.15), (4.14), (4.11) and (2.4) we find that the ring diagrams contribute the following to $\hat{S}(E, t)$:

$$\hat{S}_r(E,\epsilon) = -\mathrm{i}\bar{\rho}E^{-1}\int \mathrm{d}\boldsymbol{p}'(\boldsymbol{p}\cdot\boldsymbol{p}')\int \mathrm{d}\boldsymbol{q}\int \mathrm{d}\boldsymbol{p}_1\,\mathrm{d}\boldsymbol{p}_1'\,\mathrm{d}\boldsymbol{p}_2\,\mathrm{d}\boldsymbol{p}_2'$$
$$\times\{\langle\boldsymbol{p}|[\chi-\bar{\rho}\Lambda_0(\epsilon)]^{-1}|\boldsymbol{p}_1\rangle\langle\boldsymbol{p}_1,0|\mathscr{W}_1(\chi)|\boldsymbol{p}_2,\boldsymbol{q}\rangle$$
$$\times\left\langle\boldsymbol{p}_2\left|\frac{1}{\chi-2\boldsymbol{P}\cdot\boldsymbol{q}-\bar{\rho}\Lambda_{\boldsymbol{q}}(\epsilon)}\right|\boldsymbol{p}_2'\right\rangle$$
$$\times\langle\boldsymbol{p}_2',\boldsymbol{q}|\mathscr{W}_1(\chi)|\boldsymbol{p}_1',0\rangle\langle\boldsymbol{p}_1'|[\chi-\bar{\rho}\Lambda_0(\epsilon)]^{-1}|\boldsymbol{p}'\rangle\}\,. \tag{4.18}$$

At sufficiently low density and if $q \ll p$, $\Lambda_{\boldsymbol{q}}(\epsilon)$ can be approximated by $\Lambda_0(0^+) \equiv \Lambda$ [8]). By inspection of $\Lambda$, eq. (D.3), it is readily seen that it has the form of a classical Lorentz Boltzmann operator with an onshell quantum mechanical cross section. The problem simplifies one further step if we use S-wave interactions. In that case the matrix elements of $(\chi - 2\boldsymbol{P}\cdot\boldsymbol{q} - \bar{\rho}\Lambda)^{-1}$ can be derived explicitly, since the series one obtains by expanding this propagator in terms of the real collision part of $\Lambda$ becomes of a simple geometric nature. The complete result is given in eq. (D.4); here we will only consider the limiting form for $q$ and $\epsilon$ both small. $\Lambda$ is energy conserving so that we can split off a delta function:

$$\langle\boldsymbol{p}|(\chi-2\boldsymbol{P}\cdot\boldsymbol{q}-\bar{\rho}\Lambda)^{-1}|\boldsymbol{p}'\rangle = 2p^{-(d-2)}\delta(p^2-p'^2)\langle\hat{\boldsymbol{p}}|(\chi-2p\hat{\boldsymbol{P}}\cdot\boldsymbol{q}-\bar{\rho}\Lambda)^{-1}|\hat{\boldsymbol{p}}'\rangle\,. \tag{4.19}$$

The matrix elements at the constant energy surface are asymptotically of the following form:

$$\langle\hat{\boldsymbol{p}}|(\chi-2p\hat{\boldsymbol{P}}\cdot\boldsymbol{q}-\bar{\rho}\Lambda)^{-1}|\hat{\boldsymbol{p}}'\rangle = \mathrm{i}\omega_d^{-1}$$
$$\times\frac{(1+2\mathrm{i}\boldsymbol{p}\cdot\boldsymbol{q}\epsilon_0^{-1})(1+2\mathrm{i}\boldsymbol{p}'\cdot\boldsymbol{q}\epsilon_0^{-1})-(2\boldsymbol{p}\cdot\boldsymbol{q}\epsilon_0^{-1})^2-(2\boldsymbol{p}'\cdot\boldsymbol{q}\epsilon_0^{-1})^2+\mathcal{O}(q^3)}{[\epsilon+\gamma q^2+\mathcal{O}(q^2)]}\,. \tag{4.20}$$

$\epsilon_0$ and $\gamma$ have been defined in eqs. (2.25) and (2.26). A term due to purely imaginary collision sequences (i.e. the first term on the r.h.s. of eq. (D.4)) has been left out here, since it merely yields an exponentially decaying contribution to the VACF. The term of $\mathcal{O}(q)^2$ in the denominator is the lowest order approximation of the hydrodynamic eigen value of $(-2\mathrm{i}\boldsymbol{P}\cdot\boldsymbol{q} - \mathrm{i}\bar{\rho}\Lambda)$. The numerator is the product of two functions being the corresponding hydrodynamic mode projected along $\hat{\boldsymbol{p}}$ and $\hat{\boldsymbol{p}}'$. Several of the $\boldsymbol{p}$-integrals on the r.h.s. of eq. (4.18) can be done explicitly. In the first place we note that the momentum operator is an eigen state of $\Lambda$, so that we can replace the $\bar{\rho}\Lambda_0(\epsilon)$ terms between the braces by $\mathrm{i}\epsilon_0$, and eliminate the $\boldsymbol{p}_1$ and $\boldsymbol{p}_1'$ integrals. Secondly, because of the assumed isotropy, we only consider the virtual parts of the remaining $\mathscr{W}_1$'s, which enables us to calculate the $\boldsymbol{p}_2$ and $\boldsymbol{p}_2'$ integrals from eq. (D.1). This leads to the following expression for $\hat{S}_r(E,\epsilon)$:

$$\hat{S}_r(E,\epsilon) = \mathrm{i}\bar{\rho}E^{-1}\int \mathrm{d}\boldsymbol{q}\int \mathrm{d}\hat{\boldsymbol{p}}'\,p\epsilon_0^{-1}(E)\Bigg[\Bigg\{\langle \boldsymbol{p}|T_1(p^2-\mathrm{i}\epsilon)|\boldsymbol{p}+\boldsymbol{q}\rangle \exp\left(\frac{1}{2}\boldsymbol{q}\cdot\frac{\partial}{\partial \boldsymbol{p}}\right)$$
$$-\langle \boldsymbol{p}-\boldsymbol{q}|T_1(p^2+\mathrm{i}\epsilon)|\boldsymbol{p}\rangle \exp\left(-\frac{1}{2}\boldsymbol{q}\cdot\frac{\partial}{\partial \boldsymbol{p}}\right)\Bigg\}\left\langle \hat{\boldsymbol{p}}\left|\frac{1}{\chi-2p\hat{\boldsymbol{P}}\cdot\boldsymbol{q}-\tilde{\rho}\Lambda}\right|\hat{\boldsymbol{p}}'\right\rangle$$
$$\times\{\langle \boldsymbol{p}'+\tfrac{1}{2}\boldsymbol{q}|T_1(|\boldsymbol{p}'-\tfrac{1}{2}\boldsymbol{q}|^2-\mathrm{i}\epsilon)|\boldsymbol{p}'-\tfrac{1}{2}\boldsymbol{q}\rangle\epsilon_0^{-1}(|\boldsymbol{p}'-\tfrac{1}{2}\boldsymbol{q}|^2)(\boldsymbol{p}'-\tfrac{1}{2}\boldsymbol{q})$$
$$-\langle \boldsymbol{p}'+\tfrac{1}{2}\boldsymbol{q}|T_1(|\boldsymbol{p}'+\tfrac{1}{2}\boldsymbol{q}|^2+\mathrm{i}\epsilon)|\boldsymbol{p}'-\tfrac{1}{2}\boldsymbol{q}\rangle\epsilon_0^{-1}(|\boldsymbol{p}'+\tfrac{1}{2}\boldsymbol{q}|^2)(\boldsymbol{p}'+\tfrac{1}{2}\boldsymbol{q})\}\Bigg], \tag{4.21}$$

where $\boldsymbol{p}' \equiv |\boldsymbol{p}|\hat{\boldsymbol{p}}'$. As a consequence of the hydrodynamic property of $\Lambda$, eqs. (4.17) and (4.20), the origin of the complex $\epsilon$-plane has become a branchpoint of the left-hand cut which leads to the algebraic tail. The precise nature follows from the small $q$ behaviour of the integrand in eq. (4.21), which can be determined by a straightforward asymptotic expansion leading to a simple expression for $\hat{S}_r$

$$\hat{S}_r(E,\epsilon) \sim \int \mathrm{d}q\, q^{d-1}\left[\zeta_1(E)+\zeta_2(\epsilon)\frac{\partial}{\partial p}\right]\frac{q^2}{\epsilon+\gamma(E)q^2}, \tag{4.22}$$

or in time language

$$S_r(E,t) \sim \tfrac{1}{2}(\tfrac{3}{4}\sqrt{\pi})^{d-2}\left[\zeta_1-(\tfrac{1}{2}d+1)\left(\frac{\partial}{\partial p}\log\gamma\right)\zeta_2\right](\gamma t)^{-(d/2+1)}. \tag{4.23}$$

The denominator of eq. (4.22) is directly related to the propagator given in eq. (4.20). In the case of separable interactions the $\zeta$-functions can explicitly be worked out and are given in appendix F. The classical long-time tail is recovered if we neglect all the $q$-dependence in eq. (4.21) except in the dressed propagator. This behaviour is described by one of the terms contained in $\zeta_1$, denoted by $\zeta_{12}$, cf. eqs. (2.27) and (F.1). $\zeta_2$ and the remaining terms of $\zeta_1$ are of lower order in the density since they originate from less divergent parts of the ring diagrams. Recently however, it has been pointed out [8]) that in a quantum version of the three dimensional hard sphere system, these extra contributions may nevertheless become as important as the classical term at low energy. This also happens here, in particular we show in appendix F that the separable S-wave effective range interaction yields the same results in the low energy limit as found by Dorfman and Kirkpatrick. In fig. 7 we show the ratio, $Q(E)$, between the full long-time tail coefficient and the classical one as a function of energy at various densities. $Q(E)$ differs considerably from one at low energies. Strictly speaking the expression for $Q(E)$ is not valid for arbitrary low energies, since as already has been noted in ref. 8 the $\Lambda_q(\epsilon)\to\Lambda$ replacement is only justified if $p \gg q$ for all relevant values of $q$. This implies that

$$E > \epsilon_0(E). \tag{4.24}$$

From fig. 7 it is seen that even at energies where eq. (4.24) holds significant corrections to the classical behaviour are indeed to be expected. This follows also from the estimate of the energy region where quantum corrections are important, as we have carried out in appendix F. For a three-dimensional system the result is given by

$$E < \rho T_1(0,0)\,. \tag{4.25}$$

For two-dimensional systems this is no longer true. The logarithmic energy dependence of the $T$-matrix elements leads in that case to the following asymptotic form of $\epsilon_0$ at low energy

$$\epsilon_0(E) \sim 2\bar{\rho}\,\log^{-2}(E/\alpha^2)\,, \tag{4.26}$$

where $\alpha^{-1}$ determines the range of the interaction. Hence, eq. (4.24) becomes

$$E^2 \log^4(E/\alpha^2) > \mathcal{O}(\rho^2)\,. \tag{4.27}$$

Instead of eq. (4.25) we get

$$\left|E^2 \log^3(E/\alpha^2)\right| < \mathcal{O}(\rho^2)\,. \tag{4.28}$$

From this we see that in a two-dimensional system the quantum corrections to the long-time behaviour of the ring diagrams are expected to be small in the energy region where eq. (4.23) holds.

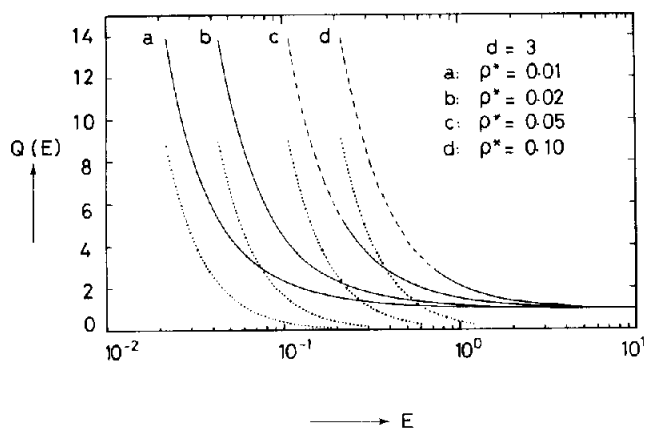


Fig. 7. Ratio of the complete long time tail coefficient generated by $\hat{S}_r$, eq. (4.21), and the classical coefficient plotted as a function of energy for various values of the density. The curves have been dashed for $E < \epsilon_0$, cf. eq. (4.24). $\rho^*$ gives the value of the scaled density as defined in table I at a chosen energy $E = 1$. The dotted line gives the asymptotic low energy behavior, as found from the ratio of the r.h.s. of eqs. (F.7) and (F.9).

## 5. Scalar inversion and semi-classical reduction of a repeated ringsum expression for $\hat{S}(E, \epsilon)$

The Dyson–Zwanzig inversion, as disussed in section 4, is not the only way to remove the naive divergences in the density expansion of the laplace transformed VACF. Instead of inverting an operator expression it is also possible to consider a scalar inversion procedure which involves matrix elements. To do so let us consider the cluster expansion of $\hat{S}(E, \epsilon)$, eq. (2.5). It can readily be seen that the cluster functions in the tetradic context are given by

$$s_n(E, \epsilon) = \frac{\mathrm{i}(2\pi)^d}{\epsilon^2 E\Omega} \langle \boldsymbol{p} | \boldsymbol{P} \bar{\mathscr{W}}_{n,\mathrm{c}} \boldsymbol{P} | \boldsymbol{p} \rangle . \tag{5.1}$$

The $\mathscr{W}_{n,\mathrm{c}}$ are the connected $n$-scatterer diagrams. The naive divergences are removed by writing $\hat{S}(E, \epsilon)$ in terms of a memory function $M(E, \epsilon)$,

$$\hat{S}(E, \epsilon) \equiv [\epsilon + M(E, \epsilon)]^{-1} . \tag{5.2}$$

$M$ is expressed in terms of the known cluster functions by making a density expansion of it

$$M(E, \epsilon) = \sum_{n=1}^{\infty} c_n(E, \epsilon) \rho^n \tag{5.3}$$

and subsequently equating the two expressions for $\hat{S}(E, \epsilon)$, which leads to

$$\begin{aligned} c_1 &= -\epsilon^2 s_1 , \\ c_n &= -\epsilon^2 s_n - \epsilon \sum_{m=1}^{n-1} s_{n-m} c_m \qquad (n \geq 2) . \end{aligned} \tag{5.4}$$

Note that the binary contribution reduces to the familiar form: $\lim_{\epsilon \to 0} \rho c_1 = \epsilon_0$, cf. (4.13).

Using this procedure we obtain the following repeated ringsum expression for the VACF:

$$\hat{S}_{\mathrm{rr}}(E, \epsilon) = [\epsilon - \mathrm{i}\bar{\rho} E^{-1} \langle \boldsymbol{p} | \boldsymbol{P} \mathscr{W}_1 \boldsymbol{P} | \boldsymbol{p} \rangle - \mathrm{i}(2\pi)^d \rho^2 E^{-1} \Omega^{-1} \langle \boldsymbol{p} | \boldsymbol{P} \mathscr{R}_{\mathrm{r}} \boldsymbol{P} | \boldsymbol{p} \rangle]^{-1} . \tag{5.5}$$

The ring operator $\mathscr{R}_{\mathrm{r}}$ has been defined in eq. (4.14).

The determination of the explicit matric elements of $\boldsymbol{P} \mathscr{R}_{\mathrm{r}} \boldsymbol{P}$ strictly parallels the derivation of eq. (4.21). By expanding the denominator in eq. (5.5) around the matrix elements of $\mathscr{R}_{\mathrm{r}}$ it is readily seen that to the leading order in the density $\hat{S}_{\mathrm{rr}}$ yields the classical negative ringsum tail. Moreover $\hat{S}_{\mathrm{rr}}$ describes the initial exponential decay of the correlation function. As a result we expect that an expression like eq. (5.5) may at least qualitatively also describe in a proper way the VACF at intermediate times. In particular we may hope to learn at what

timescale the asymptotic behaviour sets in. In order to study this, we carried out a numerical calculation of a semi-classical reduction of $\hat{S}_{rr}$. This means that we have replaced the binary term in eq. (5.5) by $\epsilon_0$. The $\Lambda_q$-operator that appears in the ring operator has been approximated by $\Lambda_0(0)$ and furthermore we have omitted the off-shell dependence of the remaining $T$-matrix elements. The light particle and the scatterers are assumed to interact via the S-wave effective range potential so that all relevant matrix elements are known explicitly, eqs. (F.6), (F.10) and (D.1). The results of this calculation are shown in figs. 8 and 9. Vertically, we have plotted the inverse Laplace transform of $\hat{S}_{rr}(E, \epsilon)$. The time variable $s$ along the horizontal axis and the scaled density $\rho^*$ have been defined according to the conventions used for the hard sphere system[4]). In table I we have summarised the definitions of $s$ and $\rho^*$ and the corresponding asymptotic behaviour of the correlation function. Fig. 8 shows $S_{rr}$ for the three dimensional case for three different values of $\rho^*$. In fig. 9 we have plotted $S_{rr}$ for the $d = 2$ case and made a comparison with the results of a molecular dynamics calculation for 2000 non-overlapping hard discs by Lewis and Tjon[15]). We have accounted for the higher order corrections to the position of the binary relaxation pole by adjusting the value of $\epsilon_0$ until an optimal fit to the short-time date was obtained. This turned out to be a 5% correction. It appears that the initial decay can be described rather well even for times when it is no longer behaving exponentially. Also the zero of the VACF is reasonably well reproduced. Our results indicate that the molecular dynamics data have not yet reached the asymptotic time region of $S_{rr}$. The shift in the long time tail coefficient produced by this effect however is

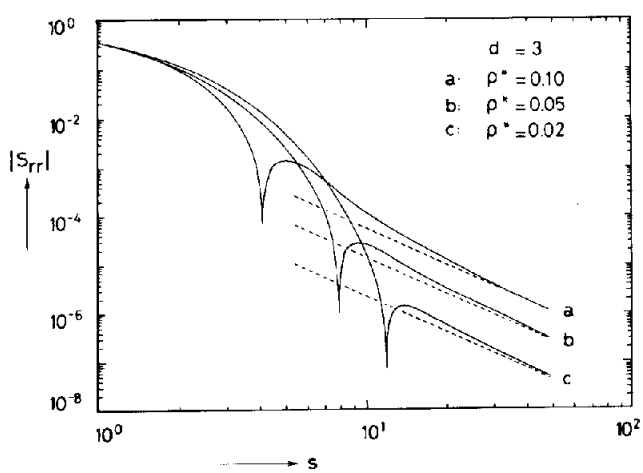


Fig. 8. Absolute value of the VACF as a function of time calculated from the repeated ringsum expression, eq. (5.5), for the three-dimensional system at various values of the density. The straight lines show the predicted asymptotic behaviour.

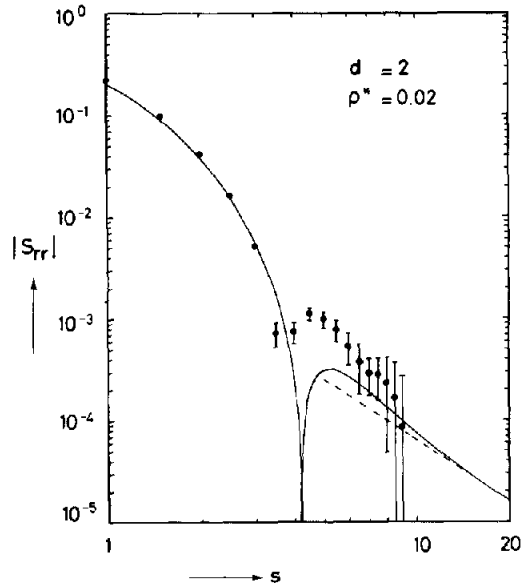


Fig. 9. As in fig. 8 for the two-dimensional case. The points show the results of a molecular dynamics calculation for 2000 nonoverlapping hard disks [15].

TABLE I
Scale convention for the two- and three-dimensional Lorentz gas. $\sigma$ is the on shell cross section $|\langle \boldsymbol{p}|T_1(p^2+\mathrm{i}0)|\boldsymbol{p}\rangle|^2$.

| $d$ | $s$ | $\rho^*$ | $S_{rr}(s\to 0)$ | $S_{rr}(s\to\infty)$ |
|---|---|---|---|---|
| 2 | $\frac{3}{4}\epsilon_0 t$ | $\dfrac{9\pi^6\sigma^2\bar{\rho}}{16E}$ | $\exp(-\frac{4}{3}s)$ | $-\dfrac{\rho^*}{\pi s^2}$ |
| 3 | $\epsilon_0 t$ | $(4\pi^2\sigma)^{3/2}\bar{\rho}$ | $\exp(-s)$ | $-\dfrac{(3\pi)^{3/2}\rho^{*2}}{16s^{5/2}}$ |

too small to explain the discrepancy between the measured and the predicted coefficient[3,5]).

## 6. Concluding remarks

We have analysed the VACF of the quantum Lorentz gas from a tetradic and a double contour approach. Although both methods are formally equivalent, there does not seem to be an obvious way to relate the corresponding diagrammatic expansions. The tetradic expressions are of a simple, classical looking, form and

the existence of a constant hydrodynamic mode is manifest. Directly related to this hydrodynamic feature is the fact that the origin of the complex $\epsilon$-plane of the Laplace transformed VACF appears to be the branchpoint of left hand cut, which leads to the algebraic long-time tails. In spite of the formal simplicity of the tetradic formalism, practical calculations are tedious. The expansion of the correlation function in terms of double Greens functions diagrams is more explicit. The classes of most divergent diagrams are given by the sum of ladders and stars but they only lead to the long-time tails in leading order of the density. For we have found out that unlike the tetradic case, the sum of these diagrams does not lead to a left-hand cut starting at the origin of the complex $\epsilon$-plane. This is only the case in leading order of the density, however the general analysis of Maleev and Toperverg[14]) indicates that the branchpoint should be shifted to the origin by including less divergent diagrams. The symmetric stars lead to the curious $t^{-(d/2)}$-tail. We have demonstrated that the corresponding $\log \epsilon$-divergence for $d = 2$ can be removed by considering the infinite class of ladders of symmetric star diagrams. On the basis of these two examples we conclude that less divergent diagrams should not be discarded a priori. In a previous letter[12]) we have argued that the hydrodynamic mode of the tetradic class of nested ring diagrams, containing the most divergent and an infinite number of less divergent diagrams, leads to a $t^{-(d/2+1)}$-tail. Hence, the physically plausible assumption that the long-time behaviour is exclusively determined by the hydrodynamic mode would imply the cancellation of the $t^{-(d/2)}$-tail as well. It should be noted however that such a dominance of the hydrodynamic mode is not in accordance with the fact that the divergences of the individual special diagrams in the tetradic analysis originate not only from the $q = 0$ but also from the $q \neq 0$ region (see e.g. eq. (E.2)), whereas this is the case in the double Greens function method. Furthermore the remaining long-time tail of the ladders of symmetric stars is not in accordance with the anticipated form if the hydrodynamic mode is dominant.

We have also considered the coefficient of the negative $t^{-(d/2+1)}$-tail which follows from the quantum-mechanical ringsum expression for the VACF. The usual way to study this quantity is by describing all intermediate, uncorrelated collisions of the ring sequence by an onshell collision operator, which is obviously not exact. For the three dimensional system there is, at low density, an overlap between the energy regions where this approximate description holds and where quantum effects become important. We have shown that this is no longer the case in two dimensions. Finally, we come to the problem of the discrepancy between the observed and predicted classical long–time coefficient. It could not be explained by the intermediate time behaviour of the VACF as we have calculated it from a semi-classical repeated ringsum expression. The double contour analysis indicates however that the asymmetric stars lead to an additional long-time tail with a coefficient that equals the ringsum result. The conclusion is based on the

comparison of the various long-time tail coefficients. Unfortunately, the model we have been considering is not suited for a rigorous calculation of the classical limit, due to the separable form of the interactions. It would be interesting to know whether this extra contribution also arises from the special diagrams in the classical analysis.

**Acknowledgements**

We thank Drs. T.R. Kirkpatrick and J.R. Dorfman for stimulating correspondence and discussion.

## Appendix A

*Double contour diagrammatics*

In this appendix we derive the diagrammatic representation of $Q_n$, eq. (2.8), which appears from the binary collision expansion of both $n$-scatterer propagators in this function. Each diagram consists out of two crosses, drawn vertically above each other, which are connected by two different arcs. On these there appear a number of dots ●, each of which represents a $T_1$-operator. The dashed line segments connect dots corresponding to the same scatterer. We associate with each $\times$ a $\boldsymbol{P}$-operator and a free propagator $G_0$ with each solid line segment —. The complex energy argument of any operator is $z_-$ resp. $z_+$ if the corresponding element of the diagram is on the left resp. the right arc. We therefore find the following rules to derive the complete binary collision expansion of $Q_n$:

1) draw all topologically different $m(=0,\ldots,n)$-scatterer diagrams, with the restriction that diagrams containing a 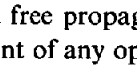 are not allowed since no two consecutive $T_1$-operators with the same scatterer index can occur;

2) label the scatterers of each diagram in an arbitrary way;

3) write down the corresponding operators by going around the diagram in clockwise direction and take the trace in the light particle Hilbert space;

4) integrate over all scatterer positions $(\boldsymbol{R}_1,\ldots,\boldsymbol{R}_m)$;

5) multiply each $m$-scatterer term with a factor $\Omega^{n-m}m!$, to account for the trivial part of the $\boldsymbol{R}^n$-integration and all scatterer permutations;

6) add all terms.

The $n$-scatterer diagrams of $Q_n$ are called connected. An index c, as used in eq. (2.9), indicates that one only has to consider the connected terms divided by a factor $n!$ which arises from the cluster expansion of the correlation function. Hence we obtain the rules for $Q_{n,c}$ from those given above by putting $m=n$ and leaving out the fifth rule.

In order to clarify the diagrammatics for the case of separable $T$-operators we write down the explicit contribution of the first diagram of fig. 1 to $s_2(E, \epsilon)$

$$a_d\Omega^{-1} \int \mathrm{d}\boldsymbol{R}_1\, \mathrm{d}\boldsymbol{R}_2\, \mathrm{Tr}[\boldsymbol{P}G_0T_1^{(1)}G_0 \cdot \boldsymbol{P}G_0T_1^{(2)}G_0T_1^{(1)}G_0T_1^{(2)}G_0]\,. \tag{A.1}$$

From eqs. (2.10), (2.12) and (2.13), it is readily seen that this expression goes over into the first term of eq. (2.15).

Finally, we consider the $n$-scatterer diagrams containing no dashed lines. From eq. (2.23) it is readily seen that the sum of all these diagrams contributes the following to the energy-dependent correlation function, $\hat{S}(E, \epsilon)$:

$$\hat{S}_\mathrm{b}(E, \epsilon) = (\pi p^d \omega_d)^{-1} \int \mathrm{d}\boldsymbol{p}'\, p'^2 [p'^2 - z_+ + \bar{\rho} T_1(p', z_+)]^{-1} \times [p'^2 - z_- + \bar{\rho} T_1(p', z_-)]^{-1}\,. \tag{A.2}$$

The asymptotic behaviour of this function for small $\rho$ and $\epsilon$ can be found to be given by

$$\hat{S}_\mathrm{b}(E, \epsilon) \sim [\epsilon + \epsilon_0(E)]^{-1}\,. \tag{A.3}$$

$\epsilon_0$ has been defined in eq. (2.26). To derive this expression one has to use the generalized optical theorem eq. (4.5) for the case of isotropic interactions,

$$\lim_{\epsilon \downarrow 0} [T_1(p, z_+) - T_1(p, z_-)] = -\mathrm{i}\pi p^{d-2}\omega_d |T_1(p, p^2 + \mathrm{i}0)|^2\,. \tag{A.4}$$

Hence, we see that these diagrams lead to an exponentially decaying contribution to the VACF, as would have been obtained from the Lorentz Boltzmann equation.

## Appendix B

*Asymptotic analysis of the dressed stars and ladders*

The explicit form of $\tilde{D}$, following from eqs. (2.12) and (2.23), is given by

$$\tilde{D}(\boldsymbol{R}, z) = \int \mathrm{d}\boldsymbol{p}' \exp(\mathrm{i}\boldsymbol{p}' \cdot \boldsymbol{R}) T_1(p', z)[z - p'^2 - \bar{\rho} T_1(p', z)]^{-1}\,. \tag{B.1}$$

Next, we apply this expression to the definition of $\tilde{U}$, eq. (2.18) and after some trivial integrations we obtain

$$\rho \tilde{U}_\epsilon(q) = \bar{\rho} \int \mathrm{d}\boldsymbol{p}'\, T_1(|\boldsymbol{p}' + \boldsymbol{q}|, z_-) T_1(p', z_+) \times \{[z_+ - p'^2 - \bar{\rho} T_1(p', z_+)][z_- - (\boldsymbol{p}' + \boldsymbol{q})^2 - \bar{\rho} T_1(|\boldsymbol{p}' + \boldsymbol{q}|, z_-]\}^{-1}\,. \tag{B.2}$$

This integral is analysed by considering the integrations over $\hat{\boldsymbol{p}}'$ and $|\boldsymbol{p}'|$ separately. For $\rho$, $\epsilon \to 0$ the $|\boldsymbol{p}'|$ contour will be pinched. The leading order behaviour of $\tilde{U}$ is determined by the residue at one of the pinching poles

$$\rho \tilde{U}_c(q) \sim \mathrm{i}\epsilon_0 \omega_d^{-1} \int \mathrm{d}\hat{\boldsymbol{p}}' [\mathrm{i}(\epsilon + \epsilon_0) + 2p\hat{\boldsymbol{p}}' \cdot \boldsymbol{q}]^{-1} . \tag{B.3}$$

For $\epsilon_0$, see eq. (2.26). Eq. (B.3) leads directly to eq. (2.24). From eq. (B.2) we see that $\rho \tilde{U}_0(0) = 1$ only if $\rho \to 0$. For the limiting form of $\tilde{L}$ we still have to analyse $\tilde{\boldsymbol{V}}$, eq. (2.21). The explicit form of this vector is given by

$$\begin{aligned} \tilde{\boldsymbol{V}}_c(\boldsymbol{q}, z_\pm) = \mathrm{i}\bar{\rho} \int \mathrm{d}\boldsymbol{p}' \, \mathrm{d}\boldsymbol{p}'' \, \delta(\boldsymbol{p}' + \boldsymbol{p}'' + \boldsymbol{q}) \boldsymbol{p}' [\epsilon + \bar{\rho} T_1(p', z_-) - \bar{\rho} T_1(p', z_+)]^{-1} \\ \times \left[ \frac{T_1(p', z_\pm)}{z_+ - p'^2 - \bar{\rho} T_1(p', z_+)} - \frac{T_1(p', z_\pm)}{z_- - p'^2 - \bar{\rho} T_1(p', z_-)} \right] \\ \times \left[ \frac{T_1(p'', z_+)}{z_+ - p''^2 - \bar{\rho} T_1(p'', z_+)} - \frac{T_1(p'', z_-)}{z_- - p''^2 - \bar{\rho} T_1(p'', z_-)} \right] . \end{aligned} \tag{B.4}$$

Again the leading order behaviour is given by the residues at the pinching poles

$$\tilde{\boldsymbol{V}}_c(\boldsymbol{q}, z_\pm) \sim 2\mathrm{i}(\tfrac{4}{3})^{d-2} \pi^2 p^d \epsilon_0^{-2} T_1(p, z_\pm) \boldsymbol{q} . \tag{B.5}$$

Combining eq. (2.24) and (B.5) we find for the dressed ladders

$$\tilde{L}(E, \epsilon) \sim -\frac{4\pi^2 E (16/9)^{d-2}}{\omega_d \epsilon_0^2 \bar{\rho}} \int \frac{\mathrm{d}q q^{d+1}}{\epsilon + \gamma q^2} , \tag{B.6}$$

which agrees with the expressions for $\zeta_{12}$ as given in eqs. (2.27) and (F.1). The long-time behaviour of the dressed stars can be determined analogously. The asymptotic form of asymmetric star contribution is given by

$$\tilde{A}_a(E, \epsilon) \sim \left( \frac{4\pi (16/9)^{d-2}}{\epsilon_0^3 \omega_d^2 p^{d-4} \sigma} \right) [T_1^2(p, z_+) + T_1^2(p, z_-)] \int \frac{\mathrm{d}q q^{d+1}}{\epsilon + \gamma q^2} . \tag{B.7}$$

The classical term is separated by rewriting the factor $[T_1^2(p, z_+) + T_1^2(p, z_-)]$ as $[T_1(p, z_+) - T_1(p, z_-)]^2 + 2|T_1(p, z_+)|^2$.

## Appendix C

*Remarks on the repeated star 4-point function and resummation of an irreducible class*

In this appendix we make some additional remarks on the mechanism by which the $t^{-1}$-tail can be removed. Firstly we derive the asymptotic form of 4-point

function of the repeated stars and after that we discuss the resummation of yet one other class of diagrams leading to a cancellation like we have shown in section 2.

In fig. 10 we show the diagrammatic representation of the 1-star 4-point function. The meaning of  has been defined in fig. 3, the external lines indicate the momenta of the light particle states between which the corresponding operators have to be sandwiched. The reduced 4-point function is obtained by leaving out the trivial $\delta(\boldsymbol{q}_+ - \boldsymbol{q}_-)$. For separable interactions, the reduced 1-star 4-point function, $X_{\boldsymbol{q}}^{(1)}(\boldsymbol{p}_-, \boldsymbol{p}_+)$, is readily found to be given by

$$X_{\boldsymbol{q}}^{(1)}(\boldsymbol{p}_-, \boldsymbol{p}_+) = \bar{\rho} \int \mathrm{d}\boldsymbol{k}[1 - \rho U_\epsilon(k)]^{-1} \delta(\boldsymbol{p}_+ + \boldsymbol{p}_- + \boldsymbol{q} + \boldsymbol{k}) \times \langle \boldsymbol{p}_- | T_1(z_-) | \boldsymbol{p}_+ \rangle \langle \boldsymbol{p}_+ + \boldsymbol{q} | T_1(z_+) | \boldsymbol{p}_- + \boldsymbol{q} \rangle . \tag{C.1}$$

In the small $k$-region $X^{(1)}$ has the following asymptotic form:

$$X_{\boldsymbol{q}}^{(1)}(\boldsymbol{p}_-, \boldsymbol{p}_+) \sim (2\pi)^d \bar{\rho} l_\epsilon \delta(\boldsymbol{p}_+ + \boldsymbol{p}_- + \boldsymbol{q}) \langle \boldsymbol{p}_- | T_1(z_-) | \boldsymbol{p}_+ \rangle \langle \boldsymbol{p}_- | T_1(z_+) | \boldsymbol{p}_+ \rangle , \tag{C.2}$$

where $l_\epsilon \sim (2\pi)^{-d} \int \mathrm{d}\boldsymbol{k}[1 - \rho U_\epsilon(k)]^{-1}$. This $l_\epsilon$ is after renormalisation asymptotically equivalent to the $l_\epsilon$ we have used in section 3, e.g. eq. (3.6). Next, we consider the $n$-star function as shown in fig. 10. The integration over the internal $\boldsymbol{q}$-variables can be carried out trivially, so that we obtain the following expression

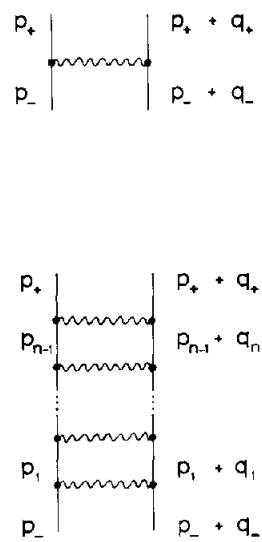


Fig. 10. 4-point functions for the 1-star and $n$-star diagrams.

for the reduced $n$-star 4-point function

$$X_q^{(n)}(p_-, p_+) = \int \mathrm{d}p^{n-1} X_q^{(1)}(p_-, p_1)[(z_- - p_1^2)(z_+ - \{p_1 + q\}^2)]^{-1} \times X_q^{(1)}(p_1, p_2) \ldots X_q^{(1)}(p_{n-1}, p_+) . \tag{C.3}$$

The asymptotic form of $X^{(n)}$ can be derived from eq. (C.2). For even $n$ we find

$$X_q^{(n)}(p_-, p_+) \sim (2\pi)^{2d} \delta(p_+ - p_-) \langle p_- | T_1(z_-) | p_+ \rangle \langle p_+ | T_1(z_+) | p_- \rangle \times [\rho l_c]^n F_4^{n/2}(p_-; q) [\hat{D}(p_-, z_-) \hat{D}(p_- + q, z_+)]^{-1} , \tag{C.4}$$

where

$$F_4(p; q) \equiv \hat{D}(p + q, z_-) \hat{D}(p + q, z_+) \hat{D}(p, z_-) \hat{D}(p, z_+) . \tag{C.5}$$

$\hat{D}$ has been defined in eq. (3.3). For odd values of $n$ we find

$$X_q^{(n)}(p_-, p_+) \sim (2\pi)^{2d} \delta(p_+ + p_- + q) \langle p_- | T_1(z_-) | p_+ \rangle \langle p_+ | T_1(z_+) | p_- \rangle \times [\rho l_c]^n F_4^{(n-1)/2}(p_-; q) . \tag{C.6}$$

Eqs. (C.4) and (C.6) yield the following asymptotic form of the repeated star 4-point function:

$$X_q(p_-, p_+) \equiv \sum_{n=1}^{\infty} X_q^{(n)}(p_-, p_+) ,$$

$$X_q(p_-, p_+) \sim \frac{(2\pi)^{2d} \langle p_- | T_1(z_-) | p_+ \rangle \langle p_+ | T_1(z_+) | p_- \rangle}{1 - (\rho l_c)^2 F_4(p_-; q)} \times \{ \delta(p_+ + p_- + q) \rho l_c + \delta(p_+ - p_-)(\rho l_c)^2 \hat{D}(p_- + q, z_-) \times \hat{D}(p_-, z_+) \} . \tag{C.7}$$

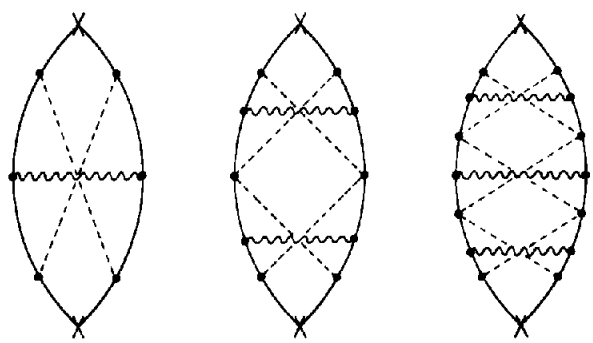

Fig. 11. Skeletons leading to the first three terms of the r.h.s. of eq. (C.8).

Since for the two-dimensional system $\tilde{l}_\epsilon = \mathcal{O}(\log \epsilon)$, the presence of a $l_\epsilon^2$ term in both numerator and denominator of the r.h.s. of eq. (C.7) indicates that the corresponding logarithmic divergence of $X^{(1)}$ is removed after resummation of the repeated stars.

We close this appendix by considering the diagrams of which the first three skeletons are shown in fig. 11. These are called irreducible since they cannot be cut in two pieces without cutting a dashed line. The contribution of this class to the energy dependent correlation function, $\hat{S}(E, \epsilon)$, is given by

$$W(E, \epsilon) = -\rho^2 a_d \Omega^{-1} \int \mathrm{d}\boldsymbol{R}_1\, \mathrm{d}\boldsymbol{R}_2 [\boldsymbol{\Pi}(\boldsymbol{R}_{12}, z_-) \cdot \boldsymbol{\Pi}(\boldsymbol{R}_{12}, z_+)] \times \sum_{n=1}^{\infty} \left\{ -\int \frac{\mathrm{d}\boldsymbol{q}}{(2\pi)^d} \frac{U_\epsilon(q)}{1 - \rho U_\epsilon(q)} \exp(\mathrm{i}\boldsymbol{R}_{12} \cdot \boldsymbol{q}) \right\}^n . \tag{C.8}$$

In this expression the related two-scatterer skeletons are included as well. It follows from eq. (2.24), that for the $d = 2$ case the $n$th term of $\tilde{W}$ is $\mathcal{O}(\rho^{n+2} \log^n \epsilon)$. The summation in eq. (C.8) can be carried out explicitly, which gives the following result for $\tilde{W}$:

$$\tilde{W}(E, \epsilon) = \rho^2 a_d \Omega^{-1} \int \mathrm{d}\boldsymbol{R}_1\, \mathrm{d}\boldsymbol{R}_2 [\tilde{\boldsymbol{\Pi}}(\boldsymbol{R}_{12}, z_-) \cdot \tilde{\boldsymbol{\Pi}}(\boldsymbol{R}_{12}, z_+)] \tilde{Y}(\boldsymbol{R}_{12}, \epsilon) , \tag{C.9}$$

where

$$Y(\boldsymbol{R}, \epsilon) = \frac{(2\pi)^{-d} \int \mathrm{d}\boldsymbol{q}\, \rho U_\epsilon(q) [1 - \rho U_\epsilon(q)]^{-1} \exp(\mathrm{i}\boldsymbol{q} \cdot \boldsymbol{R})}{\rho + (2\pi)^{-d} \mathrm{d}\boldsymbol{q}\, \rho U_\epsilon(q) [1 - \rho U_\epsilon(q)]^{-1} \exp(\mathrm{i}\boldsymbol{q} \cdot \boldsymbol{R})} . \tag{C.10}$$

From eq. (C.9) we see that the logarithmic divergences are removed by this resummation. The separate terms of the r.h.s. of eq. (C.8) can also be regularised by replacing each star in fig. 11 by a ladder of stars. The geometric progression is preserved so that this extended class can be summed explicitly as well.

## Appendix D

*Explicit formulas for the tetradic collision operators*

Each tetradic collision operator $\mathscr{W}_n$, eq. (4.3), is separated as usual into a real $\mathscr{W}_{n,\mathrm{R}}$ and a virtual $\mathscr{W}_{n,\mathrm{V}}$ part. With the help of Fano's formula, I(4.8), the explicit matrix elements are readily found

$$(\boldsymbol{p}, \boldsymbol{q} | \mathscr{W}_{n,\mathrm{V}}(\chi) | \boldsymbol{p}', \boldsymbol{q}') = \langle \boldsymbol{p} | T_n(q^2 + \chi) | \boldsymbol{p}' \rangle \delta(\boldsymbol{q} - \boldsymbol{q}') - \delta(\boldsymbol{p} - \boldsymbol{p}') \times \langle \boldsymbol{q}' | T_n(p^2 - \chi) | \boldsymbol{q} \rangle , \tag{D.1}$$

$$(\boldsymbol{p},\boldsymbol{q}|\mathscr{W}_{n,\mathrm{R}}(\chi)|\boldsymbol{p}',\boldsymbol{q}') = \oint \frac{\mathrm{d}z}{2\pi\,\mathrm{i}}\left(\frac{1}{z+\chi-p^2}-\frac{1}{z-q^2}\right)\left(\frac{1}{z+\chi-p'^2}-\frac{1}{z-q'^2}\right)$$
$$\times\langle\boldsymbol{p}|T_n(z+\chi)|\boldsymbol{p}'\rangle\langle\boldsymbol{q}'|T_n(z)|\boldsymbol{q}\rangle\,.$$

The relation with the classical Lorentz Boltzmann operator follows after applying the generalised unitarity relation, eq. (4.5), to the diagonal elements of $\mathscr{W}_n$ in the limit of $\mathrm{i}\chi \downarrow 0$:

$$\lim_{\epsilon\downarrow 0}(\boldsymbol{p},\boldsymbol{p}|\mathscr{W}_n(-\mathrm{i}\epsilon)|\boldsymbol{p}',\boldsymbol{p}') = 2\pi\,\mathrm{i}\,\delta(p^2-p'^2)$$
$$\times\left[\delta(\hat{\boldsymbol{p}}-\hat{\boldsymbol{p}}')\int \mathrm{d}\hat{\boldsymbol{p}}''\,\sigma_n(\boldsymbol{p},\boldsymbol{p}'')-\sigma_n(\boldsymbol{p},\boldsymbol{p}')\right], \tag{D.2}$$

where

$$\boldsymbol{p}' \equiv p\hat{\boldsymbol{p}}' \quad\text{and}\quad \sigma_n(\boldsymbol{p},\boldsymbol{p}') \equiv |\langle\boldsymbol{p}|T_n(p^2+\mathrm{i}0)|\boldsymbol{p}'\rangle|^2\,.$$

The limiting form of $\Lambda_0$, eq. (4.15) for isotropic interactions can be obtained at once from eq. (D.2)

$$\lim_{\epsilon\downarrow 0}\langle\boldsymbol{p}|\Lambda_0(\epsilon)|\boldsymbol{p}'\rangle = 2\pi\,\mathrm{i}|T_1(p,p^2+\mathrm{i}0)|^2\delta(p^2-p'^2)[\omega_d\delta(\hat{\boldsymbol{p}}-\hat{\boldsymbol{p}}')-1]\,, \tag{D.3}$$

where $\omega_d \equiv \int \mathrm{d}\hat{\boldsymbol{p}}$. Finally, we write down the Boltzmann propagator for the isotropic case, cf. eqs. (4.19)–(4.20),

$$\langle\boldsymbol{p}|(\chi-2p\hat{\boldsymbol{P}}\cdot\boldsymbol{q}-\bar{\rho}\Lambda)^{-1}|\hat{\boldsymbol{p}}'\rangle = \delta(\hat{\boldsymbol{p}}-\hat{\boldsymbol{p}}')(\tilde{\chi}-2\boldsymbol{p}\cdot\boldsymbol{q})^{-1}$$
$$-\frac{i\epsilon_0\omega_d^{-1}}{(\tilde{\chi}-2\boldsymbol{p}\cdot\boldsymbol{q})(\tilde{\chi}-2\boldsymbol{p}'\cdot\boldsymbol{q})}\left(1+\mathrm{i}\epsilon_0\omega_d^{-1}\int\frac{\mathrm{d}\hat{\boldsymbol{p}}''}{\tilde{\chi}-2\boldsymbol{p}''\cdot\boldsymbol{q}}\right)^{-1}, \tag{D.4}$$

where $\tilde{\chi} = -\mathrm{i}(\epsilon+\epsilon_0)$, $\epsilon_0$ has been defined in eq. (2.26).

## Appendix E

*Leading order behaviour of the first special diagram*

In this appendix we will argue that the leading order term of the three-scatterer special diagram, see fig. 6(b), is no longer strictly proportional to the fifth power

of the scattering cross section, as it would be in the classical case. The most divergent part is selected out by taking all but one of the $\mathscr{W}$-operators virtual as indicated in fig. 12. This leads to the following contribution to the memory function, eqs. (5.2)–(5.3)

$$c_{3,\mathrm{S}}(E,\epsilon) = -\mathrm{i}(2\pi)^{3d}E^{-1}\int \mathrm{d}\boldsymbol{p}'(\boldsymbol{p}\cdot\boldsymbol{p}')\int \mathrm{d}\boldsymbol{p}_1\,\mathrm{d}\boldsymbol{p}_1'\,\mathrm{d}\boldsymbol{p}_2\,\mathrm{d}\boldsymbol{p}_2'\int \mathrm{d}\boldsymbol{q}_1\,\mathrm{d}\boldsymbol{q}_2$$
$$\times[\langle \boldsymbol{p},0|\mathscr{W}_{1,\mathrm{V}}|\boldsymbol{p}_1,\boldsymbol{q}_1\rangle(\chi-2\boldsymbol{p}_1\cdot\boldsymbol{q}_1)^{-1}\langle \boldsymbol{p}_1,\boldsymbol{q}_1|\mathscr{W}_{1,\mathrm{V}}|\boldsymbol{p}_2,\boldsymbol{q}_2\rangle$$
$$\times(\chi-2\boldsymbol{p}_2\cdot\boldsymbol{q}_2)^{-1}\langle \boldsymbol{p}_2,\boldsymbol{q}_2|\mathscr{W}_{1,\mathrm{R}}|\boldsymbol{p}_2',\boldsymbol{q}_2\rangle(\chi-2\boldsymbol{p}_2'\cdot\boldsymbol{q}_2)^{-1}$$
$$\times\langle \boldsymbol{p}_2',\boldsymbol{q}_2|\mathscr{W}_{1,\mathrm{V}}|\boldsymbol{p}_1',\boldsymbol{q}_1\rangle(\chi-2\boldsymbol{p}_1'\cdot\boldsymbol{q}_1)^{-1}\langle \boldsymbol{p}_1',\boldsymbol{q}_1|\mathscr{W}_{1,\mathrm{V}}|\boldsymbol{p}',0\rangle]\,. \qquad \text{(E.1)}$$

With the help of eq. (A.1) we can integrate out the $\boldsymbol{p}_1$, $\boldsymbol{p}_2$, $\boldsymbol{p}_1'$ and $\boldsymbol{p}_2'$ variables, so that $c_{3,\mathrm{S}}$ turns out to be given as the sum of 16 terms. Only if all of these are equally divergent for $\epsilon\to 0$, the classical cross section dependence can be recovered by applying the unitarity relation to each $\mathscr{W}_{1,\mathrm{V}}$. We will now show for the two dimensional system that this is not the case. In some of the terms of $c_{3,\mathrm{S}}$ the $\boldsymbol{q}_1$- and $\boldsymbol{q}_2$-dependences factorise. If we replace the real collision operator by an energy conserving delta function, we find that these terms are proportional to the

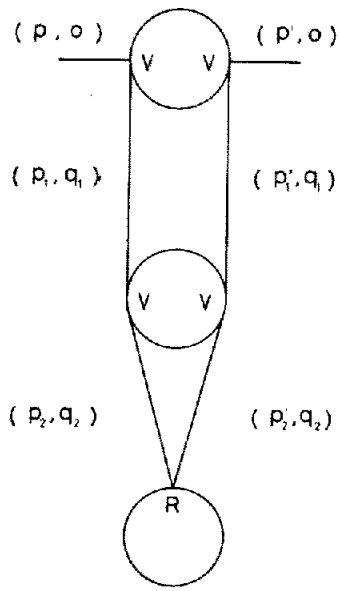


Fig. 12. Most divergent part of the three-scatterer special diagram.

following integrals:

$$f_\eta(E,\epsilon)=\int \mathrm{d}\hat{\boldsymbol{p}}'(\hat{\boldsymbol{p}}\cdot\hat{\boldsymbol{p}}')\left[\int \mathrm{d}\boldsymbol{q}(-\mathrm{i}\epsilon+2\boldsymbol{p}\cdot\boldsymbol{q}+q^2)^{-1}(-\mathrm{i}\epsilon+2\boldsymbol{p}'\cdot\boldsymbol{q}+\eta q^2)^{-1}\right]^2, \tag{E.2}$$

where $\boldsymbol{p}'=p\hat{\boldsymbol{p}}'$ and $\eta\equiv\pm 1$. The $\boldsymbol{q}$-integral can be rewritten in terms of Bessel functions by inserting a factor $(2\pi)^{-d}\int \mathrm{d}\boldsymbol{R}\int \mathrm{d}\boldsymbol{q}'\exp \mathrm{i}\boldsymbol{R}(\boldsymbol{q}-\boldsymbol{q}')$ in the $\boldsymbol{q}$-integrand and subsequently replacing $\boldsymbol{q}$ by $\boldsymbol{q}'$ in the $\eta$-dependent denominator. The result is given by

$$f_\eta(E,\epsilon)=\int \mathrm{d}\hat{\boldsymbol{p}}'(\hat{\boldsymbol{p}}\cdot\hat{\boldsymbol{p}}')\left[2\pi\eta\int_0^\infty \mathrm{d}R\, RJ_0(R|\boldsymbol{p}-\eta\boldsymbol{p}'|)\right.$$
$$\left.\times K_0(R\sqrt{-p^2-\mathrm{i}\epsilon})K_0(R\sqrt{-p^2-\mathrm{i}\eta\epsilon})\right]^2. \tag{E.3}$$

$\boldsymbol{R}$ has to be interpreted as the distance between the scatterers in fig. 11. The asymptotic form of $f_\eta(E,\epsilon)$ can be derived straightforwardly,

$$f_1(E,\epsilon)\sim \tfrac{1}{2}\pi^4E^{-1}\int \mathrm{d}\hat{\boldsymbol{p}}'(\hat{\boldsymbol{p}}\cdot\hat{\boldsymbol{p}}')(\boldsymbol{p}\cdot\boldsymbol{p}'+E+2\mathrm{i}\epsilon)^{-1}, \tag{E.4}$$

$$f_{-1}(E,\epsilon)\sim \tfrac{1}{2}\pi^4E^{-1}\int \mathrm{d}\hat{\boldsymbol{p}}'(\hat{\boldsymbol{p}}\cdot\hat{\boldsymbol{p}}')(\boldsymbol{p}\cdot\boldsymbol{p}'+E+\tfrac{1}{2}\epsilon^2E^{-1})^{-1}. \tag{E.5}$$

Hence $f_1=\mathcal{O}(\epsilon^{-1/2})$ while $f_{-1}=\mathcal{O}(\epsilon^{-1})$.

## Appendix F

### *$\zeta$-functions*

We list the explicit expressions for the $\zeta$-functions that have been defined in eq. (4.22). The second index indicates the order in $q$ of the contributing part of the numerator in eq. (4.20)

$$\zeta_{12}=-\frac{16(16/9)^{d-2}\pi^2\bar{\rho}E(\mathrm{Im}\,T_+)^2}{\epsilon_0^4\omega_d}, \tag{F.1}$$

$$\zeta_{11}=+\frac{4\pi^2(16/9)^{d-2}\bar{\rho}p(\mathrm{Im}\,T_+)\lambda g^2\,\mathrm{Re}\dfrac{\partial}{\partial p}(\epsilon_0\Delta_+)^{-1}}{\epsilon_0^2\omega_d}$$

$$-\frac{4\pi(4/3)^{d-2}\bar{\rho}(\mathrm{Im}\,T_+)(\mathrm{Re}\,T_+)}{\epsilon_0^3}$$

$$-\frac{\bar{\rho}\pi^2(16/9)^{d-2}(\mathrm{Re}\,T_+)}{p\epsilon_0\omega_d}\frac{\partial}{\partial p}[4p^2\epsilon_0^{-2}\,\mathrm{Im}\,T_+]$$

$$-\frac{4\bar{\rho}\pi^2(16/9)^{d-2}\lambda g g'(\mathrm{Re}\,\Delta_+^{-1})p(\mathrm{Im}\,T_+)}{\epsilon_0^3\omega_d}, \tag{F.2}$$

$$\zeta_{10}=\frac{\pi^2(16/9)^{d-2}\bar{\rho}(\mathrm{Re}\,T_+)}{p\epsilon_0\omega_d}\frac{\partial}{\partial p}\left[p\lambda g^2\frac{\partial}{\partial p}\,\mathrm{Re}\frac{1}{\epsilon_0\Delta_+}\right]$$

$$+\frac{\pi(4/3)^{d-2}\bar{\rho}(\mathrm{Re}\,T_+)\lambda g^2\,\mathrm{Re}\frac{\partial}{\partial p}(\epsilon_0\Delta_+)^{-1}}{p\epsilon_0}$$

$$+\frac{\pi^2(16/9)^{d-2}\bar{\rho}\lambda g g'(\mathrm{Re}\,\Delta_+^{-1})}{\epsilon_0\omega_d}\left[\lambda g^2\frac{\partial}{\partial p}\,\mathrm{Re}(\epsilon_0\Delta_+)^{-1}\right]$$

$$+\frac{2(4/3)^{d-2}\pi\bar{\rho}(\mathrm{Re}\,T_+)\lambda g g'\,\mathrm{Re}(\epsilon_0\Delta_+)^{-1}}{p\epsilon_0}, \tag{F.3}$$

$$\zeta_{21}=-\frac{4(16/9)^{d-2}\pi^2 p\bar{\rho}(\mathrm{Im}\,T_+)(\mathrm{Re}\,T_+)}{\epsilon_0^3\omega_d}, \tag{F.4}$$

$$\zeta_{20}=-\frac{\bar{\rho}(\mathrm{Re}\,T_+)}{p\epsilon_0\omega_d}\left[-\pi^2(16/9)^{d-2}p\lambda g^2\,\mathrm{Re}\frac{\partial}{\partial p}(\epsilon_0\Delta_+)^{-1}\right.$$

$$\left.-\omega_d\pi(4/3)^{d-2}\epsilon_0^{-1}(\mathrm{Re}\,T_+)\right], \tag{F.5}$$

where $T_+ = T_1(p, z_+)$ and $\Delta_+ = \Delta(z_+)$. A′ indicates differentiation to $p$. Note that the scattering information enters into the classical coefficient $\zeta_{12}$ only via cross sections. The dependence of the other coefficients on the scattering amplitudes illustrates their quantum mechanical character. The $\zeta$-function expressions (F.1)–(F.5) have been checked by calculating the long time behaviour of $S_r(E, t)$, eq. (4.18), numerically for the case of a separable S-wave effective range interaction in three dimensions. For this purpose we have considered the rate at which the discontinuity of $\hat{S}_r(E, \epsilon)$ vanishes if $\epsilon$ approaches the origin from the left and this was divided by the well-known classical rate: $\hat{S}_r^{(cl)}(E, \epsilon + i0) - \hat{S}_r^{(cl)}(E, \epsilon - i0) \sim -i\pi\zeta_{12}\gamma^{-5/2}|\epsilon|^{3/2}$. Obviously, this ratio equals $Q(E)$, cf. fig. 7. The complete discontinuity has been determined by numerically integrating at the $\hat{p}'$ and $\hat{q}$ angular dependence of the residue at the hydrodynamic pole in the complex $q$-plane for decreasing values of $|\epsilon|$.

In order to relate our results to the work of Kirkpatrick and Dorfman[8]) we consider the low energy behaviour of the $\zeta$-function for the three dimensional

system. The on shell matrix elements for the separable effective range interaction are given by the following equation (see I(3.1) and I(A.6)):

$$T_+ = a[1 + 2\pi^2 ap\,\mathrm{i} + r_0^2 p^2]^{-1}\,, \tag{F.6}$$

where $a = \lambda[2\pi^2\lambda\alpha + \alpha^2]^{-1}$ and $r_0^2 = a/\lambda$. This yields the following low-energy behaviour for the long time tail coefficients, cf. eq. (4.23):

$$\zeta_{12} \sim -16\pi^5(16/9)\frac{a^4E^2\bar{\rho}}{\epsilon_0^4}\,, \tag{F.7}$$

$$\zeta_{11} - \frac{5}{2}\left(\frac{\partial}{\partial p}\log\gamma\right)\zeta_{21} \sim -\left(\frac{112}{9}\right)\frac{\pi^3a^3p\bar{\rho}}{\epsilon_0^3}\,, \tag{F.8}$$

$$\zeta_{10} - \frac{5}{2}\left(\frac{\partial}{\partial p}\log\gamma\right)\zeta_{20} \sim -\left(\frac{56}{18}\right)\frac{\pi a^2\bar{\rho}}{E\epsilon_0^2}\,. \tag{F.9}$$

These are the (22), (12) + (21) and (11) coefficients as given in eqs. (3.14), (3.16) and (3.17) of ref. 8b. Contribution (F.9) dominates at low energy, eq. (4.25) is found by comparing eqs. (F.7) and (F.9). For the two dimensional system the $T$-matrix is of the following form

$$T_+ = \lambda[\alpha^2 + \mathrm{i}\pi^2\lambda - \pi\lambda\log(p^2/\alpha^2) + p^2]^{-1}\,. \tag{F.10}$$

The ratio between the leading contribution at low energy and the classical term is then estimated by

$$\frac{\zeta_{10} - 2\left(\frac{\partial}{\partial p}\log\gamma\right)\zeta_{20}}{\zeta_{12}} = \mathcal{O}\left(\frac{\rho^2}{E^2\log^3(p^2/\alpha^2)}\right). \tag{F.11}$$

## References


1) J.R. Dorfman, Physica **106A** (1981) 77.
E.H. Hauge, in: Lecture Notes in Physics, Vol. 31, G. Kirzenov and J. Marro, eds. (Springer, Berlin, 1974).
H. van Beijeren, Rev. Mod. Phys. **54** (1982) 195.
2) J.M.J. van Leeuwen and A. Weijland, Physica **36A** (1967) 457.
A. Weijland and J.M.J. van Leeuwen, Physica **38A** (1968) 35.
3) M.H. Ernst and A. Weijland, Phys. Lett. **34A** (1971) 39.
4) C. Bruin, Phys. Rev. Lett. **29** (1972) 1670; Physica **72** (1974) 261.
5) J.C. Lewis and J.A. Tjon, Phys. Lett. **66A** (1978) 349.
6) B.J. Alder, in: Lecture Notes in Physics, vol. 84, L. Garrido, P. Seglar and P.J. Shepard, eds. (Springer, Berlin, 1978).
B.J. Alder and W.E. Alley, J. Stat. Phys. **19** (1978) 314.
W.E. Alley and B.J. Alder, Phys. Rev. Lett. **43** (1979) 653.
7) W. Hoogeveen and J.A. Tjon, Physica **115A** (1982) 101.
8) T.R. Kirkpatrick and J.R. Dorfman, (a) J. Stat. Phys. **30** (1983) 67; (b) preprint 1983.

9) W. Hoogeveen and J.A. Tjon, Phys. Lett. **86A** (1981) 353.
10) E. Abrahams, P.W. Anderson and T.V. Ramakrishnan, Phil. Mag. **B42** (1980) 827.
L.P. Gorkov, A. Larkin and D. Khmel'nitzkii, JETP Lett. **30** (1979) 229.
D. Vollhardt and P. Wölfle, Phys. Rev. **B22** (1980) 4666.
W. Götze, P. Prelovšek and P. Wölfle, Solid State Comm. **30** (1979) 369.
P. Prelovšek, Phys. Rev. **B23** (1980) 1304.
11) T.R. Kirkpatrick and J.R. Dorfman, Phys. Rev. **A27** (1983).
12) W. Hoogeveen and J.A. Tjon, Phys. Lett. **95A** (1983) 350.
13) R. Zwanzig, Phys. Rev. **129** (1963) 486.
F.J. Dyson, Phys. Rev. **75** (1949) 486, 1736.
14) S.V. Maleev and B.P. Toperverg, Sov. Phys. JETP **42** (1976) 734.
15) J.C. Lewis and J.A. Tjon, unpublished results.